NASA Technical Paper 3546

1995

Oxidation Mechanisms of Toluene and Benzene

David A. Bittker
Lewis Research Center
Cleveland, Ohio

National Aeronautics and Space Administration

Office of Management

Scientific and Technical Information Program

1995

Oxidation Mechanisms of Toluene and Benzene

David A. Bittker
National Aeronautics and Space Administration
Lewis Research Center
Cleveland, Ohio 44135

Summary

An expanded and improved version of a previously published benzene oxidation mechanism is presented and shown to model published experimental data fairly successfully. This benzene submodel is coupled to a modified version of a toluene oxidation submodel from the recent literature. This complete mechanism is shown to successfully model published experimental toluene oxidation data for a highly mixed flow reactor and for higher temperature ignition delay times in a shock tube. A comprehensive sensitivity analysis showing the most important reactions is presented for both the benzene and toluene reacting systems. The NASA Lewis toluene mechanism's modeling capability is found to be equivalent to that of the previously published mechanism which contains a somewhat different benzene submodel.

Introduction

This report continues the investigation of aromatic hydrocarbon oxidation mechanisms begun with the development of a benzene oxidation mechanism by Bittker (1991). The increased content of aromatics in today's practical fuels makes it important to understand their oxidation chemistry because a large research effort is being devoted to the theoretical modeling of advanced concepts for high-speed, clean-burning aircraft engines. This work requires the development of simplified fuel oxidation models which realistically predict heat release rates and pollutant species emission concentrations. The latter task can only be accomplished after an understanding of the complete detailed oxidation mechanism has been obtained. Over many years of research, although steady progress has been made toward the understanding of aliphatic hydrocarbon oxidation (Warnatz (1984)), this has not been the case for aromatics. Only very recently, with the publication of the NASA Lewis benzene mechanism (Bittker, 1991) and a toluene oxidation mechanism by Emdee, Brezinsky, and Glassman (1992), has detailed modeling for experimental reactions of these fuels been reasonably successful. The latter toluene mechanism contains a benzene submodel which differs in several respects from the NASA Lewis mechanism. Both benzene oxidation mechanisms have been used to successfully compute experimental composition time profiles measured in a highly mixed flow reactor at approximately 1100 K (Lovell, Brezinsky, and Glassman, 1988). The NASA Lewis mechanism also computed with reasonable success experimental ignition delay times measured behind a reflected shock wave for lean, stoichiometric, and rich benzene-oxygen-argon mixtures (Burcat, Snyder, and Brabbs, 1986). The complete Emdee mechanism computes species profiles for the toluene oxidation which agree with experimental data measured at 1200 K in the same flow reactor used for the Lovell work.

This report first presents an improved version of the original NASA Lewis benzene oxidation mechanism. The capabilities of both mechanisms to model available experimental data are compared and sensitivity analysis results for the new mechanism are given. Differences between the Emdee and NASA Lewis mechanisms are pointed out. The NASA Lewis benzene model is then coupled with a slightly modified version of the Emdee toluene submodel. The new toluene oxidation mechanism is used to model not only the Emdee flow reactor data at 1200 K but also the ignition delay time data for toluene-oxygen-argon mixtures which were also reported by Burcat, Snyder, and Brabbs (1986). The temperature range of the Burcat data is 1300 to 1600 K; the mixture concentrations range from a lean fuel-oxygen equivalence ratio φ of 0.331 to stoichiometric ($\varphi = 1.0$). A complete sensitivity analysis is also performed to determine the rate-controlling reactions and to indicate which individual steps in the mechanism need further study.

All computations were performed with the NASA Lewis Research Center general chemical kinetics and sensitivity analysis code LSENS (Radhakrishnan, 1994, Radhakrishnan and Bittker, 1994, and Bittker and Radhakrishnan, 1994). According to the law of microscopic reversibility, all chemical reactions are considered reversible, with the ratio of the forward to reverse rates equal to the equilibrium constant. Because the net rates, therefore, depend strongly on the thermodynamic data used to compute the reaction equilibrium constants, table I lists pertinent thermodynamic data over the temperature range of interest for several important species in the benzene and toluene oxidation mechanisms. The thermodynamic data base used for most species is that of the NASA Lewis Chemical Equilibrium Composition Code (Gordon and McBride, 1994 and McBride, Reno, and Gordon (1994)). However, the table gives data for several species not in the standard data base; these data were computed recently for the present work by Bonnie J. McBride at the NASA Lewis Research Center. Data for several C_5 species were also computed by Dr. A. Burcat at Lewis. It is also important to note that the thermodynamic data for benzyl alcohol and the benzyl

radical are the same as those used by Emdee, Brezinsky, and Glassman (1992) in their computations and were provided by Dr. K. Brezinsky (1993, Princeton University, Princeton, N.J., personal communication). The exact structures of these species are not known at this time. Because their thermodynamic properties had a significant effect on the computed benzene alcohol concentration, it was important to use the same structural assumptions that Emdee, Brezinsky, and Glassman used for these molecules in their computations.

Benzene Oxidation

Chemical Mechanism

The original NASA Lewis mechanism overpredicted the formation of phenol and cyclopentadiene. Additional consumption reactions for these species were published in the benzene oxidation submodel of the Emdee toluene mechanism. These reactions and other modifications were incorporated into a new NASA Lewis benzene submodel listed in table II, which contains the three constants in the rate equation $k_j = A_j T_j^{n_j} \exp -(E_j/RT)$ for all reactions. The Emdee products and rate coefficient parameters for the reaction of oxygen atom with the cyclopentadienyl radical (C_5H_5) are now used. Instead of forming the intermediate product C_5H_5O, the reaction now forms directly the products C_4H_5 and CO. In addition, two different pyrolysis reactions of the C_4H_5 radical are used, as done in the Emdee mechanism. These are

$$C_4H_5 = C_2H_3 + C_2H_2 \qquad (50)$$

and

$$C_4H_5 + M = C_4H_4 + H + M \qquad (51)$$

The rate coefficient for reaction (50) was modified from the Emdee expression by reducing the pre-exponential factor to obtain a vinyl acetylene (C_4H_4) concentration profile consistent with the experimental results. The rate coefficient of reaction (51) was assumed to be the same as the expression used for the vinyl radical (C_2H_3) pyrolysis, reaction (60) (also done in the Emdee mechanism). In addition, destruction reactions of the species C_4H_4 and the propargyl radical (C_3H_3) were added to the NASA mechanism. The molecular pyrolysis of C_4H_4 to acetylene, suggested by Kiefer et al. (1988), was used as were reactions of vinyl acetylene with the phenyl radical and H-atom reported by Colket (1986). The reaction of C_4H_4 with the C_2H radical was reported by Frenklach et al. (1983). Abstraction reactions of the oxygen atom and the hydroxyl radical with vinyl acetylene and those of C_2H, the vinyl radical, and C_4H_5 with benzene were also used with estimated rate coefficients. Propargyl is removed by its direct reaction with molecular oxygen whose rate was measured by Slagel and Gutman (1986). Several of these reactions form 1,3 butadiene, which is removed by three reactions reported by Vaughn, Howard, and Longwell (1991). Recent discussions of benzene formation in the flames of aliphatic fuels (Miller and Melius, 1992 and Westmoreland, 1989) as well as a study of allene pyrolysis (Wu and Kern, 1987) have suggested the recombination of two propargyl radicals and the reaction of propargyl with allene as possible paths for the formation of benzene in aliphatic fuel oxidation. Several calculations with the rate coefficients given by Wu and Kern showed that these reactions had absolutely no effect on the computed results for benzene oxidation because propargyl is consumed very rapidly by its reaction with oxygen and its recombination with the H-atom to form allene. The two benzene-forming reactions were not included in the NASA mechanism. However, two additional reactions were added, both of which were used by Vaughn, Howard, and Longwell (1991) in their modeling of the benzene-ethylene-mixture oxidation in a perfectly stirred reactor:

$$C_6H_6 + CH_3 = C_6H_5 + CH_4 \qquad (10)$$

$$C_6H_5 + C_2H_2 = C_6H_5C_2H + H \qquad (11)$$

Significant formation of the product phenylacetylene was observed and measured by Vaughn, Howard, and Longwell, who used only this one reaction to model their results. In the present work, reaction (11) formed phenylacetylene near the initial reaction temperature and then destroyed it as the temperature increased toward its equilibrium combustion value.

One more point should be mentioned concerning reaction (20), the C_5H_5 abstraction of a hydrogen atom from phenol (C_6H_5OH):

$$C_5H_5 + C_6H_5OH = C_6H_5O + C_5H_6 \qquad (20)$$

The rate coefficient used in a previous work (Bittker, 1991) and in the present calculations is an estimate reported by Lovell, Brezinsky, and Glassman (1989) in their study of the pyrolysis mechanism of phenol; namely,

$$k_{20} = 2.67\times10^{14} \exp(-25200/RT) \text{ cm}^3/(\text{mole-s})$$

where R is the universal gas constant and T is the temperature in kelvin. The pre-exponential factor in this expression is rather high for this abstraction process and was replaced by another estimated expression in later work from the same research group. The latter rate coefficient was calculated from an estimate of the reverse reaction rate by means of the equilibrium constant and the law of microscopic reversibility. The expression, reported in the Emdee, Brezinsky, and Glassman (1992) paper is

$$k_{20} = 4.20\times10^{13}\, T^{-0.82} \exp(-19840/RT) \text{ cm}^3/(\text{mole-s})$$

This expression gives rate coefficient values about 2 orders of magnitude smaller than the first k_{20} given above by Lovell in 1989. However, when the new expression was used in the benzene oxidation calculations shown in the next section, insignificant differences were found from all results computed using the older expression. These differences indicate that rate coefficients computed for reaction (20) by either expression are so high that the rate of this reaction cannot have any control over the initial stage of the benzene oxidation. There may be, however, situations in which reaction (20) becomes more rate controlling. Therefore, the newer and more realistic estimated k_{20} is preferred and is listed in table II, which also includes the CH_4, C_2 hydrocarbon, and H_2 oxidation reactions used in the original NASA Lewis mechanism. All reactions are allowed to be reversible, but only the forward rate coefficient parameters are given in the table because the reverse rates are generated by LSENS at every step of the reaction as the ratio of the forward rate coefficient to the equilibrium constant. This ratio was computed internally by LSENS from Gibbs function data as described previously.

The NASA Lewis model differs from the Emdee model primarily in the products written for the reactions of molecular oxygen with the species benzene (C_6H_6) and cyclopentadiene (C_5H_6):

$$C_6H_6 + O_2 = C_6H_5O + OH \qquad (1)$$

$$C_5H_6 + O_2 = C_5H_5O + OH \qquad (22)$$

In the Emdee mechanism, these reactions are simple hydrogen atom abstractions forming HO_2 and either the C_6H_5 or the C_5H_5 radical. The above reactions, each of which could represent a two-step or more process, are an important source of OH radicals that initiate the reaction in the NASA Lewis mechanism. As discussed later in the next section, these differences in products for reactions (1) and (22) are reflected in the results of sensitivity analysis computations to determine the reactions whose rates are most controlling in the entire oxidation process.

Computational Results and Comparisons

Comparisons of computed with experimental results were made with the expanded mechanism of 146 reactions. The experimental data are the same as those used by Bittker (1991). Discussed first are the concentration profiles measured by Lovell, Brezinsky, and Glassman (1988) in a highly mixed flow reactor at 101 kPa (1 atm) and at about 1100 K. The benzene fuel was injected into a stream of nitrogen containing a low oxygen concentration and was mixed rapidly with the oxidant stream. The initial concentration and temperature conditions for the three cases reported are listed in table III as cases B-1, B-3, and B-4.

Figures 1 and 2 show the computed concentration time profiles of the four species: benzene, carbon monoxide, cyclopentadiene, and phenol from the original NASA Lewis mechanism, the new NASA mechanism, and the experimental results of Lovell, Brezinsky, and Glassman (1988). The experiments were performed at three fuel equivalence ratios φ: 0.74, 1.0, and 1.36. The time scale for the experimental concentration profiles was obtained by those authors from flow velocity measurements as a function of distance along the reactor and was corrected for the mixing time from the point of fuel injection into the oxidant stream. The flow reactor was modeled as a constant-pressure (101-kPa or 1-atm), homogeneous, static reaction. Figure 1 shows that the new mechanism changes the computed results to reduce the overall reaction speed, as indicated by the time rate of benzene consumption and carbon monoxide formation. At $\varphi = 0.74$, the new computed results deviated more from experiment than did the original ones, which already showed a slower reaction than observed experimentally. However, at the other two equivalence ratios of 1.0 and 1.36, the new results are closer to the experimental curves because the original mechanism computed faster reaction rates, as measured by the benzene and carbon monoxide profiles. In figure 2, which shows phenol and cyclopentadiene composition versus time, the important observation is that the new mechanism significantly improved the prediction of the phenol and cyclopentadiene profiles at all three equivalence ratios. The concentrations of the radicals C_6H_5O and C_5H_5 are included in the computed concentrations of phenol and cyclopentadiene, respectively, because, as explained by Emdee, Brezinsky, and Glassman (1992), these resonantly stable radicals can achieve significant concentrations and could combine with a hydrogen atom in the sampling probe and be detected as the parent species. The original NASA Lewis mechanism predicted significantly more phenol formation than was observed for all experimental conditions. With the new mechanism, agreement is very good at all three equivalence ratios. The cyclopentadiene concentration profiles computed for all conditions by the new mechanism are also in better agreement with the experimental results than were the original predictions. At the start of the reaction, the rate of increase of the C_5H_6 concentration is still faster than the experimental rate is, but the computed maximum in this species concentration is significantly reduced. Compared with the original one, the new mechanism provides a marked improvement in the prediction of experimental results, except for the benzene and CO profiles at the lean equivalence ratio. This lack of improvement for these two species is most likely because there are still unknown reactions which make both mechanisms underpredict the benzene destruction rate (and corresponding carbon monoxide formation rate) at $\varphi = 0.74$ and overpredict these rates at the other equivalence ratios.

Experimental concentration profiles of six species are given in Emdee, Brezinsky, and Glassman (1992) for an additional

benzene oxidation case in the same flow reactor. The equivalence ratio for this case is 0.91, and its initial conditions are listed as case B-2 in table III. Figure 3 shows the experimental benzene and phenol profiles for this case. Also in this figure are the computed profiles of Emdee's work as well as computed profiles using the new mechanism of the present work. For benzene, the NASA Lewis computed profile is consistent with the experimental one but is slightly lower. The computed phenol concentration is in good agreement with experiment. A comparison of the NASA Lewis computed results with those of Emdee shows that their mechanism computes an excellent match to the observed benzene results, but the NASA Lewis mechanism computes a slightly more accurate phenol profile. In figure 4 are shown experimental and computed profiles using both mechanisms for carbon monoxide and C_2 hydrocarbons, which are mostly acetylene and a small amount of ethylene. The agreement between the NASA Lewis computation and the experimental results is good, but the computation gives higher concentrations than the experiment at the start of the reaction. However, the computed and experimental concentrations are quite close at the later reaction times shown. The Emdee mechanism overestimates the C_2 formation and underestimates the carbon monoxide formation. Experimental and computed concentration profiles of cyclopentadiene and C_4 hydrocarbons (vinyl acetylene and 1,3 butadiene) are shown in figure 5. The NASA Lewis mechanism gives only a fair match to the experimental C_4 profile whereas Emdee's mechanism gives numerically close results. The trend of the Emdee curve is, however, not consistent with that of the experimental profile. Neither Emdee's nor the NASA Lewis benzene mechanism reproduces the cyclopentadiene concentration experimental profile. The NASA Lewis mechanism gives concentrations of $C_5H_5 + C_5H_6$ that are too high at early reaction times, and Emdee's computations overestimate them for the entire reaction time interval shown in the figure. Both computed curves are, however, consistent with the experimental curve at long reaction times. These comparisons illustrate the strengths and weaknesses of each mechanism.

The NASA Lewis mechanism was next tested on the prediction of the experimentally measured ignition delay times reported by Burcat, Snyder, and Brabbs (1986). Ignition was by reflected shock wave and the delay time was determined as the time (after shock passage) for observing the first significant pressure rise. For the computation, a static reaction at constant volume was assumed behind the shock, and the ignition delay time was taken as the time for a 5-percent pressure rise. Four benzene-oxygen-argon mixtures at three fuel equivalence ratios of 0.5, 1.0, and 2.0 were used in the experiments. For the stoichiometric equivalence ratio, experiments covered two conditions, a dilute (95.616 mole % argon) and a strong (85.635 mole % argon) mixture. Initial conditions for all experiments are given in table IV along with the experimental results. Table IV also lists computed ignition delay times using the new mechanism and tabulates percentage differences and percent standard deviations σ for each mixture. Ignition delay times τ computed with the new mechanism are compared with the experimental results in figures 6 to 9 for all mixtures. These figures plot $\log_{10} \tau$ versus the reciprocal of kelvin temperature T. The lines represent least-squares curve fits to the equation

$$\log_{10} \tau = \text{Constant} + \Delta E/(2.302585 \cdot RT)$$

where ΔE is an activation energy factor which is a measure of the temperature dependence of τ, and R is the universal gas constant. Comparisons show that the present mechanism predicts ignition delay times quite close to the experimental ones for the dilute mixture ($\varphi = 1.0$) and gives fair agreement for the strong mixtures ($\varphi = 0.5$ and 1.0). Agreement between experiment and calculation is poor for the $\varphi = 2.0$ mixture. Predicted ignition delay times are too long for the lean mixture and too short for both the strong stoichiometric and the rich mixtures. Similar results were shown in Bittker (1991) for the original benzene oxidation mechanism. This lack of agreement is attributed to inadequacies in both mechanisms causing them to predict too slow a reaction for $\varphi = 0.5$ and too fast a reaction for the strong stoichiometric and rich mixtures.

In view of the difficulty in defining the experimental first significant pressure rise, any σ value less than 30 percent should be considered reasonable agreement between computation and experiment. However, the present mechanism computes a weaker temperature dependence of ignition delay time than that observed experimentally for all mixtures. This fact can be seen from the slopes of the curve-fitted lines in figures 6 to 9 and also from the activation energy factors ΔE computed from these slopes and shown in table V. The computed ΔE values are between 12 and 20 percent lower than the ΔE values for the experimental curve-fitted lines.

In summary, the expanded benzene oxidation mechanism presented here has a significantly better capability of matching the available experimental concentration profile data in a flow reactor than does the original NASA Lewis mechanism. This is especially true for predicting phenol and cyclopentadiene concentration profiles at all experimental conditions. However, the new mechanism is still incomplete and has some of the same inadequacies as the original mechanism in predicting higher temperature ignition delay times. The observed differences between all experimental and predicted results will probably not be resolved until additional experimental results are available.

Sensitivity Analysis Results

The new benzene oxidation mechanism was developed with the help of detailed sensitivity analysis computations which determined the reactions whose rate coefficients had the greatest effect on computed results. Several reactions with a large uncertainty in their rate coefficients had the greatest effect on computed results when their coefficients were changed by a

moderate amount. These rate coefficients were adjusted to give the best overall agreement between computation and experiment, as shown in the previous section. Figure 10 presents normalized sensitivity coefficients for the reactions which control three concentration profiles shown in the previous section for the flow reactor case $\varphi = 0.74$. A normalized coefficient represents the approximate percent change in the variable that would be caused by a 1-percent increase in the rate coefficient of a given reaction. A negative coefficient means that increasing the rate coefficient results in a decrease in the value of the dependent variable at that reaction time. These are local sensitivity coefficients and can only give information about moderate changes in the rate coefficient. They tell nothing about the effect of large changes in the latter and, therefore, cannot predict the effect of eliminating a reaction. The information in this figure will be compared with sensitivity analysis results for the Emdee mechanism. Emdee, Brezinsky, and Glassman (1992) list the following reactions as those whose rates have the strongest effect on the benzene profile:

$$H + O_2 = OH + O \quad (130)$$

$$C_6H_5O = C_5H_5 + CO \quad (13)$$

$$C_6H_5OH = C_6H_5O + H \quad (17)$$

The rate coefficient of their direct benzene-plus-oxygen reaction (a simple H-atom abstraction) has no effect on their computed results. The situation is quite different with the present NASA Lewis mechanism.

Sensitivity coefficients for benzene and carbon monoxide concentrations are given in figures 10 (a) and (b). Reaction (1), the (chain branching) benzene reaction with molecular oxygen, is the major rate-controlling step of benzene consumption and corresponding formation of carbon monoxide. This situation is in contrast to the situation for the Emdee mechanism just noted. Reactions (13) and (17) are rate controlling in both mechanisms. The phenoxy dissociation (reaction (13)) speeds up the overall oxidation process whereas reaction (17), which proceeds in reverse to form phenol, inhibits the oxidation. The $H + O_2$ chain-branching step, which is the most rate-controlling reaction in the Emdee mechanism, ranks much lower in the NASA Lewis mechanism, below two other rate-controlling steps, reactions (6) and (22), the OH attack on benzene and the reaction of cyclopentadiene with molecular oxygen. It must be emphasized that the $H + O_2$ reaction is a very important reaction in the current mechanism, even though it is not the most rate-controlling one; because its rate is very rapid, it has a major effect on the radical pool concentrations, as it does in any hydrocarbon oxidation mechanism.

Figure 10(c) shows sensitivity coefficients for the reactions which control phenol concentration. The main rate-controlling reactions for this species are two hydroxyl radical reactions, (6) and (23). Reaction (6) increases phenol formation whereas reaction (23), the destruction of phenol by OH, decreases phenol concentration. Net rate computations show that the reverse of reaction (17) is the dominant reaction that forms phenol, but this reaction ranks significantly below the last reaction in figure 10 for controlling the phenol concentration. Reaction (1) is fourth in the sensitivity ranking for this species.

To find out what reactions are rate controlling on the ignition delay times shown in the previous section, sensitivity coefficients of pressure were computed and are shown in figure 11 for the shock ignition of the strong stoichiometric mixture at 1435 K. The same three reactions which control benzene destruction and carbon monoxide formation in the lower temperature flow reactor experiments, (1), (13), and (17), are seen to control the pressure rise in the reflected shock ignition reactions. As would be expected, they also control benzene and carbon monoxide concentration profiles computed for this ignition reaction. The $H + O_2$ chain-branching reaction is next in importance (at the higher temperature of this reaction) for controlling pressure and also carbon monoxide concentration (sensitivity coefficients not shown). This is a significant increase in its rate-controlling effect compared with its sensitivity ranking for the lower temperature flow reactor experiments.

Toluene Oxidation

Chemical Mechanism

The toluene oxidation model presented by Emdee, Brezinsky, and Glassman (1992) was added to the new benzene model just discussed. Included are 41 of the first 42 reactions in their table IV, which are reactions of toluene and its fragments. The one reaction omitted is the slower of two paths given for the reaction of the benzyl radical ($C_6H_5CH_2$) with the HO_2 radical. Computations with and without the slower process gave identical results, so it was not used. From their table, four additional reactions involving the species formaldehyde and CH_2OH were also used. Other reactions in their table were included in the new NASA benzene model. The 45 reactions in the toluene model and their rate coefficient parameters are listed in table VI. Preliminary calculations were made using all the Emdee rate coefficient parameters to compute the experimental concentration profiles for the two toluene flow reactor cases shown in the Emdee paper. The experimental conditions of Burcat, Snyder, and Brabbs (1986) were used to also compute the pressure-defined ignition delay times for toluene oxidation behind a reflected shock. Sensitivity coefficients were also computed to determine which, if any, of the Emdee rate coefficients might need adjusting to obtain the best agreement between computed and experimental results.

The preliminary sensitivity analysis showed that only five of the Emdee rate coefficients had to be adjusted to achieve the best overall agreement between the computations and all the

experimental results. In agreement with Emdee, the main rate-controlling reaction was the direct toluene-oxygen reaction

$$C_6H_5CH_3 + O_2 = C_6H_5CH_2 + HO_2 \qquad (147)$$

Because the rate coefficient of this reaction has not been measured experimentally, its pre-exponential factor was used as one of the important adjustable parameters for matching the experimental results. The value of 2.5×10^{14} given in table VI for A_{147} is only 16.7 percent lower than the Emdee value obtained by this same procedure. Two other reactions whose pre-exponential factors had to be changed from Emdee's values are the reactions of the H-atom with toluene:

$$C_6H_5CH_3 + H = C_6H_6 + CH_3 \qquad (152)$$

$$C_6H_5CH_3 + H = C_6H_5CH_2 + H_2 \qquad (153)$$

The rates of both these reactions have a significant effect on the concentration time profiles of benzene, methane, and styrene. These three species profiles were matched to the experimental results by increasing A_{152} to 25 percent above Emdee's value and decreasing A_{153} to 16.7 percent below Emdee's value. Reaction (153) also influences the cresol profile, and the decrease in its A-factor also improved this species' agreement between computed and experimental results. Only two other pre-exponential factors had to be changed from Emdee's values: these are the A-factors for the reactions

$$CH_3C_6H_4O = C_6H_6 + H + CO \qquad (157)$$

and

$$C_6H_5CH_2 + O = C_6H_5CHO + H \qquad (164)$$

Reaction (157) controls the cresoxy concentration, which controls the formation of cresols by the reaction

$$CH_3C_6H_4O + H = CH_3C_6H_4OH \qquad (156)$$

The value of A_{157} had to be decreased by 74 percent from Emdee's value to increase the computed cresol concentration level to values near those reported in the experiment. This change was justified, inasmuch as Emdee's rate coefficient expression is not an experimentally measured one. It is the expression determined experimentally by Lin and Lin (1986) for the analogous decomposition of the phenoxy radical C_6H_5O (see reaction (13) in table II). Reaction (164) is an important rate-controlling reaction for benzaldehyde. The estimated pre-exponential factor of Emdee was increased by 50 percent to give the best agreement between computed and experimental benzaldehyde concentration profiles.

In the next section are shown comparisons of the new NASA computed results with the experimental results of Emdee, Brezinsky, and Glassman and Burcat, Snyder, and Brabbs for toluene oxidation using this modified Emdee toluene mechanism coupled with the new benzene oxidation mechanism.

Computational Results and Comparisons

As indicated earlier, two sets of experimental data for high-temperature toluene oxidation were used in the development of the NASA complete oxidation mechanism. The first set consists of concentration profiles measured in the same highly mixed, atmospheric-pressure flow reactor used to obtain the benzene oxidation data described earlier in this paper. The two cases reported by Emdee, Brezinsky, and Glassman (1992) had the initial conditions given in table III as cases T-1 and T-2. Of course, the computer model of these experiments is the same as that for the benzene experiments. The second set of data consists of ignition delay times for toluene-oxygen-argon-mixture ignition behind a reflected shock wave. These data are part of the same work of Burcat, Snyder, and Brabbs (1986), who reported the benzene-oxygen ignition delay times described earlier in the section Benzene Oxidation. The pressure-rise-based ignition delay times were calculated exactly as were the ones for benzene. The flow reactor experiments are discussed first.

Figures 12 (a) and (b) present experimental concentration profiles of benzene and toluene for the lean ($\varphi = 0.69$) and rich ($\varphi = 1.33$) cases of table III, respectively. Also plotted in this figure and in figures 13 to 18 are two computed curves for each concentration profile. These are the curves using the Emdee mechanism (from their paper) and the curves using the oxidation mechanism of the present work. Figure 12 shows that both the Emdee and NASA Lewis mechanisms give excellent agreement with experiment, except for the benzene profile in the lean case for which the NASA Lewis curve is slightly low. Concentration profiles for benzaldehyde (C_6H_5CHO) and methane are presented in figure 13 for the case $\varphi = 0.69$. For each of these species, both mechanisms give good agreement with the experimentally observed trends and give fairly good quantitative agreement. The computed benzaldehyde profiles slightly over predict the experimental concentrations for early reaction times but then come into good agreement with the observed profile. The computed maximum concentration and corresponding reaction time for both computed curves are in good agreement with the experimental values, and the slopes of the computed and experimental curves are in good agreement. The NASA Lewis mechanism reproduces the experimental methane profile quite well and somewhat better than the Emdee computation, which underpredicts its concentration. Figure 14 presents experimental and computed benzyl alcohol ($C_6H_5CH_2OH$) concentrations for the same case. The agreement between computed and experimental profiles is slightly better for the Emdee mechanism. For both computed curves, the maximum concentrations are in good agreement with experiment, but the times for reaching this concentration are

too long and the observed sharp drop in concentration from the peak value is not well predicted. Figure 15 plots experimental and computed benzyl alcohol and benzaldehyde concentrations for the case $\varphi = 1.33$. Both mechanisms do a reasonably good job of predicting both profiles. The matching is better for benzyl alcohol than for benzaldehyde and the Emdee mechanism gives a more accurate maximum benzyl alcohol concentration.

Comparisons of computed and experimental concentration profiles for other species are given in figures 16 to 18. They are all for the case $\varphi = 0.69$. Figure 16 shows excellent agreement between computed and experimental carbon monoxide profiles for the NASA computed curve. Emdee's computed concentration curve for this species also matches the experimental curve quite well but shows some underprediction of the experimental results at reaction times greater than 70 ms. The acetylene concentration profiles in figure 16 show that the new mechanism consistently overpredicts acetylene concentration. At reaction times greater than 75 ms, the computed concentration is 1.5 to 2 times higher than the experimental value. By comparison, Emdee's computed acetylene profile also overpredicts the experimental results and shows much more deviation than the NASA computed curve. At reaction times greater than 75 ms, the Emdee computed acetylene concentrations are approximately three times the experimental values. Figure 17 shows that concentration profiles for phenol, ethylbenzene, and styrene are fairly well predicted by the NASA mechanism. The observed peak in phenol concentration is, however, not well predicted by the present computations. The Emdee computations predict ethylbenzene and styrene concentrations about as well as the NASA mechanism does. However, Emdee's computed phenol concentrations are significantly below the level of the experimental curve. As was done for the benzene oxidation computations, the experimental phenol concentration was compared with the sum of the computed phenol and phenoxy radical concentrations. The phenoxy concentration makes only a small contribution to the total of both concentrations. The poorest matching of experimental and computed concentration profiles is shown in figure 18 for the species cyclopentadiene and cresol. Again, the concentrations of the cresoxy and cyclopentadienyl radicals were included in the cresol and cyclopentadiene concentrations. Both are significantly underpredicted by the NASA Lewis mechanism. However, the figure shows that the NASA computed cresols curve goes through a maximum concentration value at reaction time of 120 ms, which is quite close to the experimental concentration maximum at 75 ms. Also, after a reaction time of 40 ms, the slope of the NASA computed cresol curve is about the same as that of the experimental curve. A shift in the time scale of the experimental curve would bring it into much better agreement with the computed curve. The Emdee mechanism underpredicts cresols noticeably more than the NASA Lewis mechanism does. It is interesting to note, however, that the Emdee curve for $C_5H_5 + C_5H_6$ overpredicts the measured cyclopentadiene concentration. Their computed concentration profile for C_5H_6 alone (not shown) matches the experimental curve fairly well.

The NASA toluene mechanism was next used to compute the pressure-rise-based ignition delay times for the toluene-oxygen-argon mixtures mentioned at the beginning of the Toluene Oxidation section. Both the experimental values of Burcat, Snyder, and Brabbs (1986) and the NASA computed values were obtained exactly as described previously for the shock-initiated ignitions of benzene and oxygen. Four different mixtures and two equivalence ratios ($\varphi = 0.331$ and 1.0) were used by Burcat. The mixture descriptions are given in table VII, which also tabulates the experimental and computed delay times τ and gives the same error analysis shown in table IV for the benzene ignitions. Computed and experimental ignition delay times are plotted as the $\log_{10} \tau$ versus the reciprocal of temperature for each mixture in figures 19 to 22. In each figure are plotted the actual experimental data points and the least-squares line fitted through the points. For the computations, only the least-squares-fitted lines through the computed delay times are shown. Good agreement between experimental and computed results is shown in figures 20 and 21 for mixtures 2 and 3. Both these mixtures are stoichiometric and were diluted with 95.027 mole % argon. Mixture 2 experiments had initial pressures of approximately 202 kPa (2 atm) whereas mixture 3 cases had initial pressures close to 606 kPa (6 atm). Table VII shows that the standard deviations of the computed τ values are 10.7 and 13.1 percent, respectively, for mixtures 2 and 3. Figure 19 shows that the computed τ values are significantly longer than the experimental ones for mixture 1 ($\varphi = 0.331$; initial pressures ~ 202 kPa or 2 atm). In contrast, computed τ values are much shorter than the experimental ones for mixture 4, which is stoichiometric but diluted in only 85.053-mole % percent argon. These results are shown in figure 22. Table VII gives the standard deviations of 42.1 and 36.4 percent for mixtures 1 and 4, respectively. The poor agreement for mixture 1 can be explained by the possibility of as yet undiscovered reactions which are important at the lean equivalence ratio and not at $\varphi = 1.0$. However, this explanation does not apply to the poor agreement for mixture 4. The only difference between mixtures 2 and 4 is the amount of argon dilution. The enthalpies of the mixture 4 cases at the unshocked temperature of approximately 298 K are significantly higher than those of the mixture 2 cases because of the larger fraction of fuel and oxidant in mixture 4, which also has higher heat capacity. Therefore, one would expect the initial temperature range of the mixture 4 cases to be lower than that of the mixture 2 cases for the same range of reflected shock pressure. Table VII shows that this is true. However, it is possible that these temperatures, which were computed using the idealized shock equations, are slightly high for mixture 4. A small estimated constant correction of about 0.2 percent for shock velocity attenuation was applied by this author to Burcat's original calculations of reflected shock conditions. If this correction

were greater for the higher enthalpy mixture or other deviations from ideal gas conditions became important, computed temperatures could be lowered. A modest lowering of even 1 percent (14 to 15 K) produces significantly improved agreement between computed and experimental results for the mixture 4 ignition delay times. The standard deviation of all points is reduced from 36.4 to 26.6 percent, with maximum and minimum deviations of about 34 and 15 percent for the individual data points. Also to be mentioned, as done for the benzene ignitions, is the uncertainty in determining the time of the first significant pressure rise from the experimental pressure time traces. Considering these experimental uncertainties, this comparison of computed and experimental ignition delay times raises questions that will be answered by improving the chemical mechanism and by obtaining more definitive experimental measurements of ignition delay times and other data for the oxidation of toluene at temperatures above 1300 K.

A comparison of the NASA computed temperature dependence of ignition delay and the experimental observations is shown in table VIII, which lists the activation energy factors ΔE defined for the benzene ignition delay measurements. They were computed from the slopes of the least-squares lines shown in figures 19 to 22. As in the case of benzene, the general trend is that the computed ΔE values are lower than the experimental values, in this case by about 10 to 19 percent. However, for these toluene mixtures, only three of the four are included in this trend whereas all mixtures for benzene followed the trend. Table VIII shows that the computed ΔE for the dilute and high-pressure stoichiometric mixture 3 is about 23 percent higher than the experimental value. This result is attributed to the low experimental ΔE, which is about 37 percent lower than the ΔE values for mixtures 1 and 2. Certainly, one would expect the temperature dependences of the three stoichiometric mixtures to be close to each other and also be close to that of the lean mixture. Table V shows that all benzene mixtures had about the same experimental temperature dependence. This discrepancy also shows the need for additional higher temperature data in ignition delay times for toluene-oxygen mixtures.

In summary, the NASA Lewis combined toluene-benzene oxidation mechanism presented herein accurately predicts most of the concentration profiles measured for experiments in a highly mixed flow reactor at about 1200 K. When it is used to predict ignition delay times for higher temperature (1300 to 1600 K) shock-initiated oxidations, the results are mixed. The computed pressure-based ignition delay times agree well with experimental results for some conditions but give only poor to fair agreement for other conditions. As was the case with the benzene oxidation mechanism alone, as yet undiscovered reactions must be added to the mechanism and also more experimental results are needed to resolve the discrepancies observed between the presently available experimental data and computed results, especially at temperatures above 1300 K. It should be mentioned that the Emdee mechanism also failed to give good agreement with experiment when investigators applied it to the calculation of laminar flame speeds for both benzene and toluene mixtures. Computed flame speeds for this higher temperature regime were lower than reported experimental values (Emdee, Brezinsky, and Glassman, 1992).

Sensitivity Analysis Results

Some typical results of the NASA Lewis sensitivity analysis computations performed during the development of the toluene oxidation mechanism are shown in figure 23. Sensitivity coefficients of reactions that control four species profiles are shown for case T-1 of table III, the lean-mixture toluene oxidation. The coefficients were all computed at a reaction time of 60 ms. These results are in general agreement with those of Emdee, Brezinsky, and Glassman (1992) for the reactions which control the toluene concentration profile (fig. 23(a)). The most sensitive steps are reactions (147) and (130), which have negative sensitivity coefficients and therefore promote the consumption of toluene:

$$C_6H_5CH_3 + O_2 = C_6H_5CH_2 + HO_2 \qquad (147)$$

$$H + O_2 = OH + O \qquad (130)$$

It should be mentioned that reaction (147) consumes only a small fraction of the toluene. It is a very sensitive step because it is the main source of the HO_2 radical, which is then consumed by reaction with the benzyl radical to form benzaldehyde, H, and OH radicals (reaction (176)). Net species formation rates show that reaction (176) is a primary source of the H-atom, which propagates the chain reaction destruction of toluene. Figure 23(a) also shows that HO_2 reacts with the HCO radical in reaction (118), the sixth most sensitive reaction with a negative sensitivity coefficient for toluene. Its products are molecular oxygen and formaldehyde, CH_2O, which pyrolyzes to form H-atoms and more HCO. Both products, therefore, promote the chain reaction oxidation of toluene. The next two most sensitive rate coefficients are for the reactions

$$C_6H_5CH_3 + H = C_6H_5CH_2 + H_2 \qquad (153)$$

and

$$H + C_6H_5CH_2 = C_6H_5CH_3 \qquad (148)$$

Both of these reactions proceed from left to right as written. Although reaction (153) does destroy toluene, it also forms the benzyl radical, which participates in reaction (148), the most important reaction that reforms toluene and would have an inhibiting effect on the oxidation. Figure 23(a) shows, however, that the benzyl radical also reacts with benzaldehyde in the fifth most sensitive step, reaction (187). This reaction has a negative sensitivity coefficient for toluene and, thus, an accelerating effect on the oxidation. Even though this reaction forms

toluene, the major effect of this reaction is the formation of C_6H_5CO, which rapidly dissociates to form CO and ultimately generates other free radicals that speed up fuel consumption and product formation. The net result of these competing qualitative effects in a complex mechanism usually has to be determined by a detailed sensitivity analysis. The positive sensitivity coefficient of reaction (153) in figure 23(a) shows that its overall effect is to inhibit the chain reaction process that consumes toluene. The dominance of the inhibition can be explained by the following observations. First, net-species-formation-rate calculations show that reaction (153) is the largest consumer of H-atoms. It consumes more H-atoms than the important chain-branching step, $H + O_2$, reaction (130), and so competes with it and slows down the chain oxidation of toluene. Second, the benzyl radical formed by reaction (153) speeds up reaction (148), which has two inhibiting influences: it not only consumes more H-atoms but also reforms toluene. The positive coefficient of reaction (148) is consistent with its primary effect of forming toluene. Therefore, both these reactions inhibit the oxidation process if their rate coefficient is increased. The Emdee sensitivity analysis lists the reaction

$$C_6H_5CH_3 + OH = C_6H_5CH_2 + H_2O \qquad (154)$$

as the fifth most sensitive reaction for toluene concentration and its sensitivity coefficient is positive. The present analysis also found a positive sensitivity coefficient for this reaction, but it ranks 10th in sensitivity, well below the last four reactions listed in figure 23(a). In the oxidation of aliphatic hydrocarbons, radical attacks on the fuel molecule (like reactions (153) and (154)) usually increase fuel consumption. However, both these reactions inhibit toluene consumption because of the further reaction of the benzyl radical just discussed.

The reactions that control toluene also control CO concentration, as shown by the sensitivity coefficients in figure 23(b). Reactions (130) and (147) are the most important in promoting CO formation, followed by reaction (187). Reactions (148) and (153) are the primary inhibtitors of CO formation. It should be noted that two benzene oxidation reactions are also in the group of the eight most sensitive reactions controlling both toluene and CO concentration. The first is the phenoxy dissociation (reaction (13)) which helps consume toluene and also form CO. The other is reaction (17), which reacts in the reverse direction to consume phenoxy and a hydrogen atom in forming phenol. This reaction, therefore, inhibits the oxidation process by competing for H-atoms with reaction (130), as shown by its positive sensitivity coefficient for toluene concentration and its negative coefficient for CO concentration.

Reactions (130) and (147) are dominant rate-controlling reactions in the formation of cresols and benzyl alcohol, as shown in figures 23(c) and (d), respectively. They increase the formation of both species. In figure 23(c) the next two most sensitive reactions inhibit the formation of cresols. These are reactions (153) and (154), the H and OH attacks on toluene. Note that the OH reaction is much more rate controlling on cresols than on the CO and toluene concentrations. Reaction (187) is again rate controlling and increases cresol concentration. Reaction (157), the decomposition of the cresoxy radical, is the sixth-ranked rate-controlling step. This reaction has a negative sensitivity coefficient because removing cresoxy reduces the generation of cresols by its main path, the combination of an H-atom with cresoxy (reaction (156)). These results of the sensitivity analysis led to the decreasing of the Emdee pre-exponential factor of reaction (157) to significantly increase cresol concentration without changing any other species concentrations. Although figure 23(c) shows that reaction (156) itself is the eighth-ranked controlling step, there was no attempt to increase its rate coefficient above the Emdee value. This value is already high and it would have had to have been increased by a very large amount to effect the cresol concentration significantly. This Emdee rate coefficient is essentially the value measured by He, Mallard, and Tsong (1988) for the analogous combination of the phenoxy radical with the H-atom to form phenol.

From figure 23(d), one sees that the most important reaction in controlling benzyl alcohol concentration is the principal path for its formation, reaction (165); however, the three previous sensitivity coefficient plots indicate that this is not usually the case. The rate coefficient for this recombination of the OH radical with the benzyl radical was used by Emdee, Brezinsky, and Glassman as an adjustable parameter to match the computed and experimental benzyl alcohol concentration profiles; the same procedure was used in the present work. After the rate coefficient of reaction (147) was set to obtain the best agreement with all other concentration profiles, the coefficient of reaction (165) was adjusted to give the best benzyl alcohol profile without changing any of the other concentration profiles. It is not surprising that the NASA Lewis k_{165} agreed exactly with Emdee's value, inasmuch as his thermodynamic data for the benzyl radical and the benzyl alcohol species were used. It was observed here that the attack of the OH radical on toluene, reaction (154), is the main inhibitor of benzyl alcohol formation. Reaction (153) the attack of the H-atom on the fuel, is a less sensitive reaction and is now a reaction which promotes the formation of benzyl alcohol. This reaction inhibits the formation of the three other species already discussed. The reason why reactions (153) and (154) have different effects on benzyl alcohol concentration is not clear because they both form the benzyl radical and thus help reaction (165) to form benzyl alcohol. One possibility is that the water formed in reaction (154) is much less reactive than the molecular hydrogen formed in reaction (153). This example shows again that it is not always clear what the effect of changing a given reaction rate coefficient will be in a complex system, and a detailed sensitivity analysis needs to be done.

To find out which reaction rates control the computed toluene oxidation ignition delay times presented in the previous section, the sensitivity coefficients of pressure were calculated

for the present toluene mechanism. Typical results are given in figure 24 for the case $\varphi = 0.331$ at an initial temperature of 1334 K. The reaction time of 700 ms is about 200 ms before the ignition delay time. The same reactions which control the flow reactor oxidation experiments can be seen to control the shock ignitions at the higher temperatures (and pressures). The pressure rise is controlled mainly by reactions (130) and (147) and is inhibited by the H and OH attacks on the fuel, reactions (153) and (154). The dissociation-recombination reactions of phenol and phenoxy from the benzene oxidation mechanism also influence the rate of pressure rise. Although not shown, the sensitivity analysis results for toluene concentration give the same reaction rankings as those shown for pressure.

In summary, the sensitivity analysis findings were in general agreement with the results of Emdee, Brezinsky, and Glassman (1992) but differed in some details. The two primary rate-controlling steps were the direct toluene-oxygen reaction and the $H + O_2$ radical chain-branching step. The inhibiting toluene + OH reaction was less controlling on the toluene and also CO concentration profiles than Emdee found. In the NASA Lewis mechanism, the reaction of benzaldehyde with benzyl, reaction (187), was a significant rate-controlling step. It promoted the consumption of fuel and the corresponding formation of CO. The present analysis also showed that two benzene mechanism reactions had a noticeable effect on the computed concentration and pressure rise profiles in toluene oxidation.

Conclusions

This report presented an expanded NASA Lewis benzene oxidation mechanism which has improved capability to match most experimental concentration profiles. This mechanism was compared with that developed by Emdee, Brezinsky, and Glassman and differs from it in several respects. The two mechanisms were comparable in computing published experimental concentration profiles. For example, the Emdee mechanism predicted more accurate benzene and C_4 hydrocarbon profiles whereas the NASA Lewis mechanism gave more accurate CO, phenol, and C_2 hydrocarbon profiles. Neither mechanism predicted the cyclopentadiene concentration profile very well. The NASA Lewis mechanism also did a reasonable job of computing higher temperature and pressure experimental ignition delay times. A modified version of the Emdee toluene oxidation mechanism was coupled to the NASA Lewis benzene mechanism. A few of the Emdee rate coefficients had to be modified because of differences between the two benzene submodels. The NASA Lewis complete model was used to compute not only Emdee's toluene experimental data but also to match higher temperature and pressure toluene oxidation ignition delay times. Comparisons of computed results for both complete toluene models with experimental data showed that each was equally good in matching the experiments. Both had successes and failures in reproducing the experimental results. When the NASA Lewis predictions of toluene oxidation concentration profiles were compared with those of the Emdee mechanism, several species concentrations were predicted equally well. However, Emdee matched the experimental benzyl alcohol profiles better than the NASA Lewis mechanism did; the NASA Lewis matched the experimental methane profile better than Emdee did. Although both mechanisms predicted more acetylene production than observed experimentally, the NASA computed curve was noticeably closer to the experimental one. Also, the NASA Lewis computed phenol concentration profile agreed much better with the experimental results than did Emdee's, which was well below the experimental curve. Both mechanisms had difficulty computing the experimental cresol concentration profile. One major difference between the two mechanisms was their computed concentration profiles of cyclopentadiene. The NASA Lewis mechanism predicted too low concentrations of this species and the Emdee mechanism, too high levels.

When both benzene and toluene oxidation mechanisms (Emdee and NASA Lewis) were applied to matching experimental data taken at temperatures above 1200 K, mixed results were obtained, indicating that they both lacked important, as yet undetermined reactions needed to fully explain high-temperature experimental results. The Emdee mechanism computed laminar flame speeds which are lower than values reported in the literature for both benzene and toluene flames. In the present work, both benzene and toluene mechanisms gave only mediocre agreement when used to compute experimental ignition delay times for oxidations behind a reflected shock. These mechanisms must be applied to new high-temperature experimental results as they become available to obtain a complete oxidation mechanism for both fuels. It is also clear that several uncertain reaction rate coefficients for key steps in these mechanisms need to be measured.

In conclusion, both the NASA Lewis and Emdee models for toluene and benzene oxidation are comparable in predicting the presently available experimental data for these fuels.

Lewis Research Center
National Aeronautics and Space Administration
Cleveland, Ohio, May 31, 1995

References

Bittker, D.A.: Detailed Mechanism for Oxidation of Benzene. Combust. Sci. Technol., vol. 79, 1991, pp. 49–72.

Bittker, D.A.: Errata for Detailed Mechanism for Oxidation of Benzene. Combust. Sci. Technol., vol. 86, 1992, p. 337.

Bitter, D.A.; and Radhakrishnan, K.: LSENS—A General Chemical Kinetics and Sensitivity Analysis Code for Homogeneous Gas-Phase Reactions, Part III: Illustrative Test Problems. NASA RP–1330, 1994.

Böehland, T.; Temps, F.; and Wagner, H. Gg.: Kinetics of the Reactions of CH_2 Radicals With C_2H_2 and C_4H_2 in the Temperature Range 296 K ≤ T ≤ 700K. Twenty-First Symposium (International) on Combustion, The Combustion Institute, Pittsburgh, 1986, pp. 841–850.

Brabbs, T.A.; and Brokaw, R.S.: Shock Tube Measurements of Specific Reaction Rates in the Branched Chain CH_4-CO-O_2 System. Fifteenth Symposium (International) on Combustion, The Combustion Institute, Pittsburgh, 1974, pp. 893–901.

Brabbs, T.A.; and Musiak, J.D.: Ignition Delay Time Measurements and Proposed Kinetic Model for Hydrogen-Oxygen. NASP CR–1030, Nov. 1988.

Braun-Unkhoff, M.; Frank, P.; and Just, Th.: A Shock Tube Study on the Thermal Decomposition of Toluene and of the Phenyl Radical at High Temperatures. Twenty-Second Symposium (International) on Combustion, The Combustion Institute, Pittsburgh, 1988, pp. 1053–1061.

Burcat, A.; Snyder, C.; and Brabbs, T.A.: Ignition Delay Times for Benzene and Toluene With Oxygen in Argon Mixtures. NASA TM–87312, 1986.

Cherian, M.A., et al.: Kinetic Modelling of the Oxidation of Carbon Monoxide in Flames. Eighteenth Symposium (International) on Combustion, The Combustion Institute, Pittsburgh, 1981, pp. 385–396.

Colket III, M.B.: The Pyrolysis of Acetylene and Vinyl Acetylene in a Single-Pulse Shock Tube. Twenty-First Symposium (International) on Combustion, The Combustion Institute, Pittsburgh, 1986, pp. 851–864.

Dean, A.M.: Detailed Kinetic Modeling of Autocatalysis in Methane Pyrolysis. J. Phys. Chem., vol. 94, pp. 1432–1439.

Emdee, J.L.; Brezinsky, K.; and Glassman, I.: A Kinetic Model for the Oxidation of Toluene Near 1200 K. J. Phys. Chem., vol. 96, 1992, pp. 2151–2161.

Fahr, A.; and Stein, S.E.: Reactions of Vinyl and Phenyl Radicals With Ethyne, Ethene and Benzene. Twenty-Second Symposium (International) on Combustion, The Combustion Institute, Pittsburgh, 1988, pp. 1023–1029.

Frank, P.; Bhaskaran, K.A.; and Just, Th.: Acetylene Oxidation: the Reaction C_2H_2 + O at High Temperatures. Twenty-First Symposium (International) on Combustion, The Combustion Institute, Pittsburgh, 1986, pp. 885–893.

Frenklach, M., et al.: Soot Formation in Shock-Tube Pyrolysis of Acetylene, Allene and 1,3 Butadiene. Combust. Flame, vol. 54, 1983, pp. 81–101.

Gordon, S.; and McBride, B.J.: Computer Program for Calculation of Complex Chemical Equilibrium Compositions and Applications: I. Analysis. NASA RP–1311, 1994.

He, Y.Z.; Mallard, W.G.; and Tsang, W.: Kinetics of Hydrogen and Hydroxyl Radical Attack on Phenol at High Temperatures. J. Phys. Chem., vol. 92, 1988, pp. 2196–2201.

Hsu, D.S.Y.; Lin, C.Y.; and Lin, M.C. : CO Formation in Early Stage High Temperature Benzene Oxidation Under Fuel Lean Conditions: Kinetics of the Initiation Reaction, $C_6H_6 = C_6H_5 + H$. Twentieth Symposium (International) on Combustion, The Combustion Institute, Pittsburgh, 1984, pp. 623–660.

Kiefer, J.H., et al.: Unimolecular Dissociation of Vinylacetylene: A Molecular Reaction. J. Phys. Chem., vol. 92, 1988, pp. 677–685.

Kiefer, J.H., et al.: A Shock Tube Investigation of Major Pathways in the High-Temperature Pyrolysis of Benzene. J. Phys. Chem., vol. 89, 1985, pp. 2013–2019.

Lin, Chin-Y.; and Lin, M.C.: Thermal Decomposition of Methyl Phenyl Ether in Shock Waves: The Kinetics of Phenoxy Radical Reactions. J. Phys. Chem., vol. 90, 1986, pp. 425–431.

Lin, C-Y.; and Lin, M.C.: Kinetics of the Phenyl Radical + Molecular Oxygen Reaction. Combustion Institute, Eastern Section, Twentieth Fall Technical Meeting, 1987, pp. 7–1 to 7–3.

Lovell, A.B.; Brezinsky, K.; and Glassman, I.: Benzene Oxidation Perturbed by Nitrogen Dioxide Addition. Twenty-Second Symposium (International) on Combustion, The Combustion Institute, Pittsburgh, 1988, pp. 1063–1074.

Lovell, A.B.; Brezinsky, K.; and Glassman, I.: The Gas Phase Pyrolysis of Phenol. Int. J. Chem. Kinet, vol. 21, 1989, pp. 547–560.

Madronich, S.; and Felder, W.: Kinetics and Mechanism of the Reaction of OH with C_6H_6 Over 790-1410 K. J. Phys. Chem., vol. 89, 1985, pp. 3556–3561.

McBride, B.J.; Reno, M.A.; and Gordon, S.: CET93 and CETPC: An Interim Updated Version of the NASA Lewis Computer Program for Calculating Complex Chemical Equilibria With Applications. NASA TM–4557, 1994.

McLain, A.G.; Jachimowski, C.J.; and Wilson, C.H.: Chemical Kinetic Modeling of Benzene and Toluene Oxidation Behind Shock Waves. NASA TP-1472, 1979.

Miller, J.A.; and Melius, C.F.: Kinetic and Thermodynamic Issues in the Formation of Aromatic Compounds in Flames of Aliphatic Fuels. Combust. Flame, vol. 91, 1992, pp. 21–39.

Miller, J.A., et al.: Toward a Comprehensive Chemical Kinetic Mechanism for the Oxidation of Acetylene: Comparison of Model Predictions With Results From Flame and Shock Tube Experiments. Nineteenth Symposium (International) on Combustion, The Combustion Institute, Pittsburgh, 1982, pp. 181–196.

Nicovich, J.M.; Gump, C.A.; and Ravishankara, A.R.: Rates of Reactions of $O(^3P)$ With Benzene and Toluene. J. Phys. Chem., vol. 86, 1982, pp. 1684–1690.

Pamidimukkala, K.M., et al.: High-Temperature Pyrolysis of Toluene. J. Phys. Chem., vol. 91, 1987, pp. 2148–2154.

Radhakrishnan, K.: LSENS—A General Chemical Kinetics and Sensitivity Analysis Code for Homogeneous Gas-Phase Reactions, Part I: Theory and Numerical Solution Procedures. NASA RP–1328, 1994.

Radhakrishnan, K; and Bittker, D.A.: LSENS—A General Chemical Kinetics and Sensitivity Analysis Code for Homogeneous Gas-Phase Reactions, Part II: Code Description and Usage. NASA RP–1329, 1994.

Slagle, I.R. et al.: Kinetics of Polyatomic Free Radicals Produced by Laser Photolysis 3. Reaction of Vinyl Radicals With Molecular Oxygen. J. Am. Chem. Soc., vol. 106, 1984, pp. 4356–4361.

Slagle, I.R.; and Gutman, D.: Kinetics of the Reaction of C_3H_3 With Molecular Oxygen from 293–900 K. Twenty-First Symposium (International) on Combustion, The Combustion Institute, Pittsburgh, 1986, pp. 875–883.

Vaughn, C.B.; Howard, J.B.; and Longwell, J.P.: Benzene Destruction in Fuel-Rich Jet-Stirred Reactor Combustion, Combust. Flame, vol. 87, 1991, pp. 278–288.

Warnatz, J.: Rate Coefficients in the C/H/O System. Combust. Chem., Gardiner, W.C., Jr. ed., Springer-Verlag, New York, 1984, pp. 197–360.

Westbrook, C.K.; and Dryer, F.L.: Chemical Kinetic Modeling of Hydrocarbon Combustion. Prog. Energy Combust. Sci. vol. 10, 1984, pp. 1–57.

Westley, F.: Table of Recommended Rate Constants for Chemical Reactions Occurring in Combustion. NSRDS-NBS–67, National Bureau of Standards, Washington, D.C., 1980.

Westmoreland, P.R., et al.: Forming Benzene in Flames by Chemically Activated Isomerization. J. Phys. Chem., vol. 93, 1989, pp. 8171–8180.

Wu, C.H.; and Kern, R.D.: Shock-Tube Study of Allene Pyrolysis, J. Phys. Chem., vol. 91, 1987, pp. 6291–6296.

TABLE I.—THERMODYNAMIC DATA FOR REACTING SPECIES

Parameter	Species					
	Phenol C_6H_5OH	Phenoxy C_6H_5O	Benzene C_6H_6	Phenyl C_6H_5	Cyclopentadienolyl C_5H_4OH	Cyclopentadienonyl C_5H_5O
(a) Thermodynamic data at 298.15 K						
Heat capacity, C_p, cal/mole-K	24.789	22.566	19.629	18.873	22.130	21.516
Enthalpy, $\Delta_f H$, kcal/mole	−23.034	11.404	19.792	78.503	19.150	19.300
Entropy, $S°$, cal/mole-K	75.329	73.570	64.308	68.914	73.150	73.541

(b) Heat capacity C_p and entropy $S°$ at various temperatures, cal/mole-K

Temperature, T, K	C_p	$S°$	C_p	$S°$	C_p	$S°$	C_p	$S°$	C_p	$S°$	C_p	$S°$
400	32.388	83.705	29.766	81.234	26.924	71.121	25.453	75.403	28.819	80.617	28.050	80.796
600	43.685	99.134	40.611	95.501	38.099	84.293	35.527	87.756	38.505	94.285	37.938	94.182
1000	55.571	124.61	52.169	119.33	50.419	107.02	46.590	108.84	48.285	116.54	48.052	116.23
1200	58.679	135.02	55.087	129.10	53.624	116.51	49.420	117.60	50.789	125.57	50.679	125.23
1400	61.261	144.27	57.497	137.78	56.278	124.98	51.761	125.40	52.820	133.56	52.823	133.21
1600	63.381	152.59	59.462	145.59	58.448	132.64	53.671	132.44	54.443	140.72	54.548	140.38
1800	65.097	160.16	61.041	152.69	60.197	139.63	55.208	138.85	55.717	147.21	55.916	146.88
2000	66.465	167.09	62.288	159.19	61.585	146.05	56.424	144.73	56.699	153.13	56.981	152.83

TABLE I.—Continued. THERMODYNAMIC DATA FOR REACTING SPECIES

Parameter	Species					
	Cyclopentadiene C_5H_6	Cyclopentadienyl C_5H_5	Butadiene C_4H_6	Butadienyl C_4H_5	Ketyl radical C_2HO	Ketene C_2H_2O
(a) Thermodynamic data at 298.15 K						
Heat capacity, C_p, cal/mole-K	18.041	18.309	19.020	18.317	10.803	12.367
Enthalpy, $\Delta_f H$, kcal/mole	31.935	63.500	26.109	76.007	38.500	−11.401
Entropy, $S°$, cal/mole-K	65.495	66.798	66.630	70.585	58.956	57.814

(b) Heat capacity C_p and entropy $S°$ at various temperatures, cal/mole-K

Temperature, T, K	C_p	$S°$	C_p	$S°$	C_p	$S°$	C_p	$S°$	C_p	$S°$	C_p	$S°$
400	24.646	71.744	24.686	73.099	24.606	73.016	23.224	76.678	11.716	62.265	14.215	61.717
600	34.697	83.768	33.484	84.925	32.746	84.663	30.253	87.529	13.068	67.282	16.885	68.020
1000	45.794	104.42	42.690	104.48	41.467	103.70	37.697	104.97	15.243	74.490	20.245	77.509
1200	48.682	113.03	45.402	112.51	44.073	111.49	39.724	112.03	16.089	77.347	21.356	81.303
1400	51.060	120.72	47.412	119.67	46.033	118.45	41.346	118.28	16.767	79.880	22.205	84.662
1600	52.992	127.67	48.925	126.10	47.413	124.69	42.626	123.89	17.302	82.155	22.855	87.671
1800	54.540	134.01	50.081	131.94	48.497	130.34	43.619	128.97	17.723	84.218	23.359	90.393
2000	55.761	139.82	50.977	137.26	49.354	135.50	44.378	133.60	18.057	86.104	23.752	92.875

TABLE I.—Continued. THERMODYNAMIC DATA FOR REACTING SPECIES

Parameter	Species					
	Toluene C_7H_8	Benzyl $C_6H_5CH_2$	Benzyl alcohol $C_6H_5CH_2OH$	Cresols $CH_3C_6H_4OH$	Ethyl benzene $C_6H_5C_2H_5$	Styrene $C_6H_5C_2H_3$
(a) Thermodynamic data at 298.15 K						
Heat capacity, C_p, cal/mole-K	24.684	26.082	26.389	30.599	30.449	28.726
Enthalpy, $\Delta_f H$, kcal/mole	11.991	50.311	−24.000	−31.620	7.151	35.445
Entropy, $S°$, cal/mole-K	76.527	76.753	80.069	86.072	86.193	82.402

(b) Heat capacity C_p and entropy $S°$ at various temperatures, cal/mole-K

Temperature, T, K	C_p	$S°$	C_p	$S°$	C_p	$S°$	C_p	$S°$	C_p	$S°$	C_p	$S°$
400	33.105	84.970	34.030	85.550	35.745	89.144	39.439	96.326	40.348	96.535	37.943	92.193
600	46.927	101.16	46.468	101.86	51.061	106.71	53.077	115.07	56.774	116.18	52.521	110.48
1000	62.452	129.19	60.224	129.20	67.559	137.12	67.964	146.09	75.117	149.98	68.269	141.43
1200	66.668	140.96	63.928	140.52	71.928	149.84	72.016	158.85	80.155	164.14	72.433	154.26
1400	70.114	151.50	66.954	150.61	75.500	161.21	75.336	170.21	84.230	176.82	75.822	165.69
1600	72.895	161.05	69.393	159.71	78.382	171.48	78.021	180.45	87.522	188.29	78.543	176.00
1800	75.105	169.77	71.331	168.00	80.673	180.85	80.162	189.77	90.146	198.75	80.695	185.38
2000	76.833	177.78	72.845	175.60	82.466	189.45	81.843	198.31	92.206	208.36	82.369	193.97

TABLE I.—Concluded. THERMODYNAMIC DATA FOR REACTING SPECIES

Parameter	Species		
	Cresoxy $CH_3C_6H_4O$	Benzaldehyde C_6H_5CHO	Hydroxyl OH
(a) Thermodynamic data at 298.15 K			
Heat capacity, C_p, cal/mole-K	27.605	26.719	7.166
Enthalpy, $\Delta_f H$, kcal/mole	2.820	−8.793	9.318
Entropy, $S°$, cal/mole-K	83.302	80.289	43.881

(b) Heat capacity C_p and entropy $S°$ at various temperatures, cal/mole-K

Temperature T, K	C_p	$S°$	C_p	$S°$	C_p	$S°$
400	36.188	92.635	34.967	89.323	7.089	45.975
600	49.870	110.05	47.497	106.04	7.058	48.839
1000	65.214	139.56	60.939	133.89	7.332	52.493
1200	69.204	151.82	64.287	145.31	7.565	53.851
1400	72.434	162.74	67.051	155.43	7.775	55.033
1600	75.006	172.58	69.30	164.54	7.962	56.084
1800	77.020	181.54	71.105	172.81	8.128	57.032
2000	78.563	189.74	72.528	180.37	8.275	57.896

TABLE II.—BENZENE OXIDATION SUBMECHANISM

Number	Reaction	Forward rate coefficients			Reference
		A_j, cm^3, mole, s	n_j	E_j, cal/mole	
1	$C_6H_6 + O_2 \rightharpoonup C_6H_5O + OH$	4.0×10^{13}	0	34 000	Bittker (1991)
2	$C_6H_6 + C_6H_5 \rightharpoonup C_{12}H_{10} + H$	4.0×10^{11}		4 000	Fahr and Stein (1988)
3	$C_6H_6 \rightharpoonup C_6H_5 + H$	5.0×10^{15}		108 000	Hsu, Lin, and Lin (1984)[a]
4	$C_6H_6 + H \rightharpoonup C_6H_5 + H_2$	2.5×10^{14}		16 000	Kiefer et al. (1985)
5	$C_6H_6 + O \rightharpoonup C_6H_5O + H$	2.78×10^{13}		4 910	Nicovich, Gump, and Ravishankara (1982)
6	$C_6H_6 + OH \rightharpoonup C_6H_5 + H_2O$	2.13×10^{13}		4 580	Madronich and Felder (1985)
7	$C_6H_6 + C_2H \rightharpoonup C_6H_5 + C_2H_2$	1.0×10^{13}		0	Estimated
8	$C_6H_6 + C_2H_3 \rightharpoonup C_6H_5 + C_2H_4$	1.0×10^{13}		0	Estimated
9	$C_6H_6 + C_4H_5 \rightharpoonup C_6H_5 + C_4H_6$	1.0×10^{13}		10 000	Estimated
10	$C_6H_6 + CH_3 \rightharpoonup C_6H_5 + CH_4$	4.365×10^{-4}	5.0	12 300	Pamidimukkala et al. (1987)
11	$C_6H_5 + C_2H_2 \rightharpoonup C_6H_5C_2H + H$	3.24×10^{11}	0	1 350	Vaughn, Howard, and Longwell (1991)
12	$C_4H_3 + M \rightharpoonup C_4H_2 + H + M$	1.0×10^{16}		60 000	Miller et al. (1982)
13	$C_6H_5O \rightharpoonup C_5H_5 + CO$	2.51×10^{11}		43 900	Lin and Lin (1986)
14	$C_6H_5 + O_2 \rightharpoonup C_6H_5O + O$	2.1×10^{12}		7 470	Lin and Lin (1987)
15	$C_6H_5 + HO_2 \rightharpoonup C_6H_5O + OH$	2.0×10^{13}		1 000	Bittker (1991)
16	$C_6H_5 \rightharpoonup C_4H_3 + C_2H_2$	4.5×10^{13}		72 530	Braun-Unkhoff, Frank, and Just (1988)
17	$C_6H_5OH \rightharpoonup C_6H_5O + H$	2.0×10^{16}		88 000	Bittker (1991)
18	$C_6H_5OH + H \rightharpoonup C_6H_6 + OH$	2.2×10^{13}		7 910	Lovell, Brezinsky, and Glassman (1989)
19	$C_6H_5OH + H \rightharpoonup C_6H_5O + H_2$	1.15×10^{14}		12 405	Lovell, Brezinsky, and Glassman (1989)
20	$C_5H_5 + C_6H_5OH \rightharpoonup C_6H_5O + C_5H_6$	4.20×10^{13}	−0.82	19 840	Emdee, Brezinsky, and Glassman (1992)[b]
21	$C_5H_6 \rightharpoonup C_5H_5 + H$	8.13×10^{24}	−2.98	78 682	Dean (1990)
22	$C_5H_6 + O_2 \rightharpoonup C_5H_5O + OH$	1.0×10^{13}	0	20 712	Bittker (1991)
23	$C_6H_5OH + OH \rightharpoonup C_6H_5O + H_2O$	3.0×10^{13}		0	Bittker (1991)
24	$C_6H_5OH + HO_2 \rightharpoonup C_6H_5O + H_2O_2$	3.0×10^{13}		1 500	Bittker (1991)
25	$C_6H_5OH + O \rightharpoonup C_6H_5O + OH$	2.81×10^{13}		7 352	Emdee, Brezinsky, and Glassman (1992)
26	$C_6H_5OH + C_2H_3 \rightharpoonup C_6H_5O + C_2H_4$	6.0×10^{12}		0	
27	$C_6H_5OH + C_4H_5 \rightharpoonup C_6H_5O + C_4H_6$	6.0×10^{12}		0	
28	$C_6H_5OH + C_6H_5 \rightharpoonup C_6H_5O + C_6H_6$	4.91×10^{12}		4 400	
29	$C_5H_6 + OH \rightharpoonup C_5H_5 + H_2O$	3.43×10^{9}	1.18	−447	
30	$C_5H_6 + H \rightharpoonup C_5H_5 + H_2$	2.19×10^{8}	1.77	3 000	
31	$C_5H_6 + O \rightharpoonup C_5H_5 + OH$	1.81×10^{13}	0	3 080	
32	$C_5H_6 + C_2H_3 \rightharpoonup C_5H_5 + C_2H_4$	6.0×10^{12}		0	
33	$C_5H_6 + C_4H_5 \rightharpoonup C_5H_5 + C_4H_6$	6.0×10^{12}		0	
34	$C_4H_6 \rightharpoonup C_4H_5 + H$	1.2×10^{16}		109 910	Vaughn, Howard, and Longwell (1991)
35	$C_4H_6 + OH \rightharpoonup C_4H_5 + H_2O$	4.79×10^{12}		1 230	Vaughn, Howard, and Longwell (1991)
36	$C_4H_6 + H \rightharpoonup C_4H_5 + H_2$	1.51×10^{14}		10 200	Vaughn, Howard, and Longwell (1991)
37	$C_5H_6 + HO_2 \rightharpoonup C_5H_5 + H_2O_2$	1.99×10^{12}		11 600	Emdee, Brezinsky, and Glassman (1992)
38	$C_5H_5O \rightharpoonup C_4H_5 + CO$	3.0×10^{16}		15 000	Bittker (1991)
39	$C_5H_5 + O \rightharpoonup C_4H_5 + CO$	1.0×10^{14}		0	Emdee, Brezinsky, and Glassman (1992)
40	$C_5H_5 + OH \rightharpoonup C_5H_4OH + H$	1.0×10^{13}		0	Bittker (1991)
41	$C_5H_4OH \rightharpoonup C_4H_4 + HCO$	1.0×10^{15}		22 000	Bittker (1991)
42	$C_4H_4 + C_6H_5 \rightharpoonup C_6H_6 + C_4H_3$	1.0×10^{12}		0	Colket (1986)
43	$C_4H_4 \rightharpoonup 2\ C_2H_2$	1.3×10^{15}		82 500	Kiefer et al. (1988)
44	$C_4H_4 + O \rightharpoonup C_4H_3 + OH$	1.0×10^{13}		0	Estimated
45	$C_4H_4 + OH \rightharpoonup C_4H_3 + H_2O$	1.0×10^{13}		0	Estimated
46	$C_4H_4 + H \rightharpoonup C_4H_3 + H_2$	1.6×10^{14}		14 500	Colket (1986)
47	$C_4H_4 + C_2H \rightharpoonup C_4H_3 + C_2H_2$	4.0×10^{13}		0	Frenklach et al. (1983)
48	$C_5H_5 + HO_2 \rightharpoonup C_5H_5O + OH$	2.0×10^{13}		0	Bittker (1991)

[a]Adjustment of A-factor to 1.0×10^{16} for increased pressure (approx) from Kiefer et al. (1985) used for ignition delay time computations.

[b]See discussion of this rate coefficient in the section Benzene Oxidation.

TABLE II.—Continued. BENZENE OXIDATION SUBMECHANISM

Number	Reaction	Forward rate coefficients			Reference
		A_j, cm^3, mole, s	n_j	E_j, cal/mole	
49	$2\ C_6H_5 \rightharpoonup C_{12}H_{10}$	3.1×10^{12}	0	0	Bittker (1991)
50	$C_4H_5 \rightharpoonup C_2H_3 + C_2H_2$	2.0×10^{11}	0.7	42 260	(c)
51	$C_4H_5 + M \rightharpoonup C_4H_4 + H + M$	3.0×10^{15}	0	32 000	Est. from reaction (60)
52	$C_4H_2 + O \rightharpoonup C_2HO + C_2H$	1.0×10^{13}		0	McLain, Jachimowski, and Wilson (1979)
53	$C_4H_2 + OH \rightharpoonup C_3H_2 + HCO$	3.0×10^{13}		0	Miller et al. (1982)
54	$C_4H_2 + O \rightharpoonup CO + C_3H_2$	1.2×10^{12}		0	Miller et al. (1982)
55	$C_2H_4 + M \rightharpoonup C_2H_2 + H_2 + M$	9.33×10^{16}		77 200	Miller et al. (1982)
56	$C_2H_4 + OH \rightharpoonup C_2H_3 + H_2O$	4.79×10^{12}		1 230	Westbrook and Dryer (1984)
57	$C_2H_4 + O \rightharpoonup CH_3 + HCO$	3.31×10^{12}		1 130	
58	$C_2H_4 + O \rightharpoonup CH_2O + CH_2$	2.51×10^{13}		5 000	
59	$C_2H_4 + OH \rightharpoonup CH_3 + CH_2O$	2.0×10^{12}		960	
60	$C_2H_3 + M \rightharpoonup C_2H_2 + H + M$	3.0×10^{15}		32 000	Warnatz (1984)
61	$C_2H_3 + O_2 \rightharpoonup CH_2O + HCO$	3.98×10^{12}		−250	Slagle et al. (1984)
62	$C_2H_3 + H \rightharpoonup C_2H_2 + H_2$	6.0×10^{12}		0	Miller et al. (1982)
63	$C_2H_3 + OH \rightharpoonup C_2H_2 + H_2O$	5.00×10^{12}			
64	$C_2H_3 + CH_2 \rightharpoonup C_2H_2 + CH_3$	3.00×10^{13}			
65	$C_2H_3 + C_2H \rightharpoonup 2\ C_2H_2$	3.00×10^{13}			
66	$C_2H_3 + O \rightharpoonup C_2H_2O + H$	3.30×10^{13}			
67	$CH_2 + CH_2 \rightharpoonup C_2H_2 + H_2$	4.00×10^{13}			
68	$CH_2 + CH_2 \rightharpoonup C_2H_3 + H$	5.00×10^{12}			Westbrook and Dryer (1984)
69	$CH_2 + OH \rightharpoonup CH + H_2O$	2.51×10^{11}	0.67	25 700	Miller et al. (1982)
70	$CH_2 + O \rightharpoonup CH + OH$	2.00×10^{11}	.68	25 000	
71	$CH + O_2 \rightharpoonup CO_2 + 2H$	1.59×10^{12}	0	1 000	
72	$C_2H_2 + M \rightharpoonup C_2H + H + M$	4.17×10^{16}		107 000	
73	$C_2H_2 + C_2H_2 \rightharpoonup C_4H_3 + H$	2.00×10^{12}		45 900	
74	$C_2H_2 + C_2H \rightharpoonup C_4H_2 + H$	3.00×10^{13}		0	
75	$C_2H_2 + O \rightharpoonup CH_2 + CO$	1.60×10^{14}		9 890	Frank, Bhaskaran, and Just (1986)
76	$C_2H_2 + O \rightharpoonup C_2HO + H$	4.00×10^{14}		10 660	Frank, Bhaskaran, and Just (1986)
77	$C_2H_2 + OH \rightharpoonup C_2H + H_2O$	6.31×10^{12}		7 000	Westbrook and Dryer (1984)
78	$C_2H_2 + OH \rightharpoonup C_2H_2O + H$	3.20×10^{11}		200	Westbrook and Dryer (1984)
79	$C_2H_2 + CH_2 \rightharpoonup C_3H_3 + H$	1.20×10^{13}		6 600	Boehland, Temps, and Wagner (1986)
80	$C_3H_4 + M \rightharpoonup C_3H_3 + H + M$	2.00×10^{17}		65 000	Pamidimukkala et al. (1987)
81	$C_3H_3 + O_2 \rightharpoonup C_2H_2O + HCO$	3.00×10^{10}		2 870	Slagle and Gutman (1986)
82	$C_2H_2O + OH \rightharpoonup CH_2O + HCO$	2.80×10^{13}		0	Miller et al. (1982)
83	$C_2H_2O + OH \rightharpoonup C_2HO + H_2O$	7.50×10^{12}		3 000	Miller et al. (1982)
84	$C_2H_2O + H \rightharpoonup CH_3 + CO$	1.13×10^{13}		3 428	Westbrook and Dryer (1984)
85	$C_2H_2O + H \rightharpoonup C_2HO + H_2$	7.50×10^{13}		8 000	Miller et al. (1982)
86	$C_2H_2O + O \rightharpoonup C_2HO + OH$	5.00×10^{13}		8 000	
87	$C_2H_2O + O \rightharpoonup CH_2O + CO$	2.00×10^{13}		0	
88	$C_2H_2O + M \rightharpoonup CH_2 + CO + M$	2.00×10^{16}		60 000	
89	$C_2HO + O_2 \rightharpoonup 2\ CO + OH$	1.46×10^{12}		2 500	
90	$C_2HO + O \rightharpoonup 2\ CO + H$	1.20×10^{12}		0	Westbrook and Dryer (1984)
91	$C_2HO + OH \rightharpoonup 2\ HCO$	1.00×10^{13}		0	Miller et al. (1982)
92	$C_2HO + H \rightharpoonup CH_2 + CO$	5.00×10^{13}		0	
93	$C_2HO + CH_2 \rightharpoonup C_2H_3 + CO$	3.00×10^{13}		0	
94	$C_2HO + CH_2 \rightharpoonup CH_2O + C_2H$	1.00×10^{13}		2 000	
95	$2\ C_2HO \rightharpoonup C_2H_2 + 2\ CO$	1.00×10^{13}		0	
96	$C_2H + OH \rightharpoonup C_2HO + H$	2.00×10^{13}		0	

[c]Modified from Emdee, Brezinsky, and Glassman (1992) by reducing A-factor.

TABLE II.—Continued. BENZENE OXIDATION SUBMECHANISM

Number	Reaction	Forward rate coefficients			Reference
		A_j, cm^3, mole, s	n_j	E_j, cal/mole	
97	$C_2H + O_2 \rightarrow C_2HO + O$	5.00×10^{13}	0	1 500	Miller et al. (1982)
98	$C_2H + O \rightarrow CO + CH$	5.00×10^{13}		0	Miller et al. (1982)
99	$CH_4 + M \rightarrow CH_3 + H + M$	2.00×10^{17}		88 000	Westbrook and Dryer (1984)
100	$CH_4 + O_2 \rightarrow CH_3 + HO_2$	7.94×10^{13}		56 000	Westbrook and Dryer (1984)
101	$CH_4 + H \rightarrow CH_3 + H_2$	1.26×10^{14}		11 900	Brabbs and Brokaw (1974)
102	$CH_4\ OH \rightarrow CH_3 + H_2O$	2.50×10^{13}		5 010	Brabbs and Brokaw (1974)
103	$CH_4 + O \rightarrow CH_3 + OH$	1.90×10^{14}		11 720	Brabbs and Brokaw (1974)
104	$CH_3 + O_2 \rightarrow CH_3O + O$	4.79×10^{13}		29 000	Westbrook and Dryer (1984)
105	$CH_3 + OH \rightarrow CH_3O + H$	6.30×10^{12}		0	Westley (1980)
106	$CH_3O + M \rightarrow CH_2O + H + M$	5.00×10^{13}		21 000	Westbrook and Dryer (1984)
107	$CH_3O + O_2 \rightarrow CH_2O + HO_2$	1.00×10^{12}		6 000	
108	$CH_3O + H \rightarrow CH_2O + H_2$	2.00×10^{13}		0	
109	$CH_3 + CH_3 \rightarrow C_2H_4 + H_2$	1.00×10^{16}		32 000	
110	$CH_3 + O \rightarrow CH_2O + H$	1.29×10^{14}		2 000	
111	$CH_3 + CH_2O \rightarrow CH_4 + HCO$	1.00×10^{10}	0.5	6 000	
112	$CH_3 + HCO \rightarrow CH_4 + CO$	3.00×10^{11}	0.5	0	
113	$CH_3 + HO_2 \rightarrow CH_3O + OH$	2.00×10^{13}	0	0	
114	$CH_2O + M \rightarrow H + HCO + M$	5.00×10^{16}		76 500	Warnatz (1984)
115	$CH_2O + OH \rightarrow HCO + H_2O$	3.00×10^{13}		1 200	
116	$CH_2O + H \rightarrow HCO + H_2$	2.50×10^{13}		3 990	
117	$CH_2O + O \rightarrow HCO + OH$	3.50×10^{13}		3 510	
118	$HCO + HO_2 \rightarrow CH_2O + O_2$	1.00×10^{14}		3 000	Westley (1980)
119	$HCO + M \rightarrow H + CO + M$	2.94×10^{14}		15 569	Cherian et al. (1981)[d]
120	$HCO + O_2 \rightarrow CO + HO_2$	3.31×10^{12}		7 000	Westbrook and Dryer (1984)
121	$HCO + OH \rightarrow CO + H_2O$	1.00×10^{14}		0	
122	$HCO + H \rightarrow CO + H_2$	2.00×10^{14}			
123	$HCO + O \rightarrow CO + OH$	1.00×10^{14}			
124	$CH + O_2 \rightarrow HCO + O$	1.00×10^{13}			
125	$CO + O + M \rightarrow CO_2 + M$	5.90×10^{15}		4 100	
126	$CO + O_2 \rightarrow CO_2 + O$	2.50×10^{12}		47 690	
127	$CO + OH \rightarrow CO_2 + H$	4.17×10^{11}		1 000	Brabbs and Brokaw (1974)
128	$CO + HO_2 \rightarrow CO_2 + OH$	5.75×10^{13}		22 930	Westbrook and Dryer (1984)
129	$O + H_2O \rightarrow OH + OH$	6.80×10^{13}		18 365	Brabbs and Musiak (1988)
130	$H + O_2 \rightarrow OH + O$	1.89×10^{14}		16 400	
131	$O + H_2 \rightarrow OH + H$	4.20×10^{14}		13 750	
132	$H + HO_2 \rightarrow H_2 + O_2$	7.28×10^{13}		2 126	
133	$O + HO_2 \rightarrow OH + O_2$	5.00×10^{13}		1 000	
134	$HO_2 + OH \rightarrow H_2O + O_2$	8.00×10^{12}		0	
135	$H + HO_2 \rightarrow OH + OH$	1.34×10^{14}		1 070	

[d]Computed from reverse rate coefficient and equilibrium constant.

Collisional Efficiencies

Reaction (140): $H_2 = 2.3$; $O_2 = 0.78$; $H_2O = 6.0$; $H_2O_2 = 6.6$

Reaction (142): $H_2 = 3.0$; $O_2 = 1.3$; $H_2O = 21.3$; $N_2 = 1.3$; $CO_2 = 7.0$; $C_6H_6 = 20.0$; $CH_4 = 5.0$

Reaction (143): $H_2 = 4.0$; $O_2 = 1.5$; $H_2O = 20.0$; $N_2 = 1.5$; $CO_2 = 4.0$; $C_6H_6 = 20.0$

Reaction (145): $H_2 = 4.1$; $O_2 = 2.0$; $H_2O = 15.0$; $N_2 = 2.0$

TABLE II.—Concluded. BENZENE OXIDATION SUBMECHANISM

Number	Reaction	Forward rate coefficients			Reference
		A_j, cm^3, mole, s	n_j	E_j, cal/mole	
136	$H_2 + HO_2 \rightharpoonup H_2O_2 + H$	7.91×10^{13}	0	25 000	Brabbs and Musiak (1988)
137	$OH + H_2O_2 \rightharpoonup H_2O + HO_2$	6.10×10^{12}		1 430	
138	$HO_2 + HO_2 \rightharpoonup H_2O_2 + O_2$	1.80×10^{12}		0	
139	$H + H_2O_2 \rightharpoonup OH + H_2O$	7.80×10^{11}		0	
140	$H_2O_2 + M \rightharpoonup OH + OH + M$	1.44×10^{17}		45 510	
141	$H_2 + OH \rightharpoonup H_2O + H$	4.74×10^{13}		6 098	
142	$H + O_2 + M \rightharpoonup HO_2 + M$	1.46×10^{15}		−1 000	
143	$H_2O + M \rightharpoonup H + OH + M$	1.30×10^{15}		105 140	
144	$O + H + M \rightharpoonup OH + M$	7.10×10^{18}	−1.0	0	
145	$H_2 + M \rightharpoonup H + H + M$	2.20×10^{14}	0	96 000	
146	$O_2 + M \rightharpoonup O + O + M$	1.80×10^{18}	−1.0	118 020	

TABLE III.—INITIAL CONDITIONS FOR OXIDATION OF BENZENE AND TOLUENE IN FLOW REACTOR AT 101 kPa (1 atm)

Case number	Fuel	Mixture concentrations, ppmv			Temperature, T, K	Equivalence ratio,[a] φ
		Fuel	Oxygen	Nitrogen		
B–1	Benezene[b]	1571	15 900	982 529	1098	0.74
B–2	Benzene[c]	1495	12 301	986 204	1096	0.91
B–3	Benzene[b]	1591	11 700	986 709	1096	1.0
B–4	Benzene[b]	1581	8 700	989 719	1096	1.36
T–1	Toluene[c]	1540	20 015	978 445	1188	0.69
T–2	Toluene[c]	1616	10 907	987 477	1190	1.33

[a](Fuel-oxygen mole ratio)/(stoichiometric fuel-oxygen mole ratio).

[b]Lovell, Brezinsky, and Glassman (1988).

[c]Emdee, Brezinsky, and Glassman (1992).

TABLE IV.—COMPARISON OF COMPUTED AND EXPERIMENTAL IGNITION DELAY TIMES FOR BENZENE OXIDATION BEHIND A REFLECTED SHOCK

Mixture number and description	Initial temperature, T, K	Ignition delay time, τ, μs		Percentage difference
		Experimental	Computed	
1	1209	878	870	−0.9
Equivalence ratio, φ, 0.5	1227	743	721	−3.0
Mole % argon, 78.333	1254	435	524	20.5
Pressure, p, kPa (atm)	1276	330	416	26.1
≅ 190.9 to 231.4	1291	272	360	32.4
(1.890 to 2.291)	1314	202	282	39.6
	1345	159	210	32.1
	----	---	---	[a]26.1
2	1345	755	750	−0.7
Equivalence ratio, φ, 1.0	1374	604	570	−5.6
Mole % argon, 95.616	1402	415	450	8.4
Pressure, p, kPa (atm)	1412	412	413	0.2
≅ 573.1 to 720.5	1428	367	358	−2.4
(5.674 to 7.134)	1482	213	230	8.0
	1525	122	161	32.0
	1528	122	158	29.5
	----	---	---	[a]16.1
3	1283	750	530	−29.3
Equivalence ratio, φ, 1.0	1290	613	496	−19.1
Mole % argon, 85.635	1294	607	466	−23.2
Pressure, p, kPa (atm)	1328	490	330	−32.7
≅ 205.5 to 250.5	1355	303	260	−14.2
(2.035 to 2.480)	1369	287	232	−19.4
	1379	291	211	−27.5
	1405	198	170	−14.1
	1408	189	164	−13.2
	1417	178	153	−14.0
	1435	151	127	−15.9
	----	---	---	[a]21.3
4	1363	1520	690	−54.6
Equivalence ratio, φ, 2.0	1415	890	458	−48.5
Mole % argon, 93.553	1457	599	312	−47.9
Pressure, p, kPa (atm)	1540	274	168	−38.7
≅ 202.6 to 265.3	1554	243	150	−38.3
(2.006 to 2.627)	1570	211	132	−37.4
	1582	157	123	−21.7
	1600	154	107	−30.5
	----	---	---	[a]40.9

[a]Standard deviation, σ.

TABLE V.—TEMPERATURE DEPENDENCE OF IGNITION DELAY TIMES FOR BENZENE OXIDATION BEHIND A REFLECTED SHOCK

Mixture number and description	Activation energy factor, ΔE, cal	
	Experimental	Computed
1 Equivalence ratio, φ, 0.5 Pressure, p, kPa (atm) ≅ 202 (2)	42 718	33 949
2 Equivalence ratio, φ, 1.0 (dilute) Pressure, p, kPa (atm) ≅ 606 (6)	41 472	34 828
3 Equivalence ratio, φ, 1 (strong) Pressure p, kPa (atm) ≅ 202 (2)	37 251	33 649
4 Equivalence ratio, φ, 2.0 Pressure, p, kPa (atm) ≅ 202 (2)	42 404	34 264

TABLE VI.—TOLUENE OXIDATION SUBMECHANISM

Number	Reaction	Coefficients in the equation $k = A_j T^{n_j} \exp(E_j/RT)$			Reference
		A_j, cm^3, mole, s	n_j	E_j, cal/mole	
147	$C_6H_5CH_3 + O_2 \rightharpoonup C_6H_5CH_2 + HO_2$	2.50×10^{14}	0	41 400	This work
148	$H + C_6H_5CH_2 \rightharpoonup C_6H_5CH_3$	1.80×10^{14}		0	Emdee, Brezinsky, and Glassman (1992)
149	$C_6H_5CH_3 \rightharpoonup C_6H_5 + CH_3$	1.40×10^{16}		99 800	
150	$C_6H_5 + C_6H_5CH_3 \rightharpoonup C_6H_6 + C_6H_5CH_2$	2.10×10^{12}		4 400	
151	$CH_3 + C_6H_5CH_3 \rightharpoonup C_6H_5CH_2 + CH_4$	3.16×10^{11}		9 500	
152	$C_6H_5CH_3 + H \rightharpoonup C_6H_6 + CH_3$	1.50×10^{13}		5 148	This work
153	$C_6H_5CH_3 + H \rightharpoonup C_6H_5CH_2 + H_2$	1.00×10^{14}		8 235	This work
154	$C_6H_5CH_3 + OH \rightharpoonup C_6H_5CH_2 + H_2O$	1.26×10^{13}		2 583	Emdee, Brezinsky, and Glassman (1992)
155	$C_6H_5\ CH_3 + O \rightharpoonup CH_3C_6H_4O + H$	1.63×10^{13}		3 418	Emdee, Brezinsky, and Glassman (1992)
156	$CH_3C_6H_4O + H \rightharpoonup CH_3C_6H_4OH$	2.50×10^{14}		0	Emdee, Brezinsky, and Glassman (1992)
157	$CH_3C_6H_4O \rightharpoonup C_6H_6 + H + CO$	6.50×10^{10}		43 900	This work
158	$CH_3C_6H_4OH + OH \rightharpoonup CH_3C_6H_4O + H_2O$	6.00×10^{12}		0	Emdee, Brezinsky, and Glassman (1992)
159	$CH_3C_6H_4OH + H \rightharpoonup CH_3C_6H_4O + H_2$	1.15×10^{14}		12 400	
160	$CH_3C_6H_4OH + H \rightharpoonup C_6H_5CH_3 + OH$	2.21×10^{13}		7 910	
161	$CH_3C_6H_4OH + H \rightharpoonup C_6H_5OH + CH_3$	1.20×10^{13}		5 148	
162	$CH_3C_6H_4OH + C_6H_5CH_2 \rightharpoonup CH_3C_6H_4O + C_6H_5CH_3$	1.05×10^{11}		9 500	
163	$C_6H_5CH_2 + O \rightharpoonup C_6H_5\ CHO + H$	3.75×10^{14}		0	This work
164	$C_6H_5CH_2 + O \rightharpoonup C_6H_5 + CH_2O$	8.00×10^{13}		0	Emdee, Brezinsky, and Glassman (1992)
165	$C_6H_5CH_2 + OH \rightharpoonup C_6H_5CH_2OH$	6.00×10^{13}		0	
166	$C_6H_5CH_2OH + O_2 \rightharpoonup C_6H_5CHO + H + HO_2$	2.00×10^{14}		41 400	
167	$C_6H_5CH_2OH + H \rightharpoonup C_6H_6 + CH_2OH$	1.20×10^{13}		5 148	
168	$C_6H_5CH_2OH + OH \rightharpoonup C_6H_5CHO + H + H_2O$	8.43×10^{12}		2 583	
169	$C_6H_5CH_2OH + H \rightharpoonup C_6H_5CHO + H + H_2$	8.00×10^{13}		8 235	
170	$C_6H_5CH_2OH + C_6H_5CH_2 \rightharpoonup C_6H_5CHO + C_6H_5CH_3 + H$	2.11×10^{11}		9 500	
171	$C_6H_5CH_2OH + C_6H_5 \rightharpoonup C_6H_5CHO + C_6H_6 + H$	1.40×10^{12}		4 400	
172	$CH_3 + OH \rightharpoonup CH_2OH + H$	1.09×10^{11}	0.40	−708	
173	$CH_2OH + O_2 \rightharpoonup CH_2O + HO_2$	2.41×10^{14}	0	5 000	
174	$CH_2OH + M \rightharpoonup CH_2O + H + M$	1.67×10^{24}	−2.5	34 190	
175	$CH_2O + HO_2 \rightharpoonup HCO + H_2O_2$	1.99×10^{12}	0	11 600	
176	$C_6H_5CH_2 + HO_2 \rightharpoonup C_6H_5CHO + H + OH$	2.50×10^{14}	0	0	
177	$2\ C_6H_5CH_2 \rightharpoonup$ bibenzyl	2.51×10^{11}	0.4	0	
178	$C_6H_5C_2H_5 \rightharpoonup C_6H_5CH_2 + CH_3$	2.00×10^{15}	0	72 700	
179	$C_6H_5C_2H_5 + OH \rightharpoonup C_6H_5C_2H_3 + H + H_2O$	8.43×10^{12}		2 583	
180	$C_6H_5C_2H_5 + H \rightharpoonup C_6H_5C_2H_3 + H + H_2$	8.00×10^{13}		8 235	
181	$C_6H_5C_2H_5 + O_2 \rightharpoonup C_6H_5C_2H_3 + H + HO_2$	2.00×10^{14}		41 400	
182	$C_6H_5CHO + O_2 \rightharpoonup C_6H_5CO + HO_2$	1.02×10^{13}		38 950	
183	$C_6H_5CHO + OH \rightharpoonup C_6H_5CO + H_2O$	1.71×10^{9}	1.18	−447	
184	$C_6H_5CHO + H \rightharpoonup C_6H_5CO + H_2$	5.00×10^{13}	0	4 928	
185	$C_6H_5CHO + H \rightharpoonup C_6H_6 + HCO$	1.20×10^{13}	0	5 148	
186	$C_6H_5CHO + O \rightharpoonup C_6H_5CO + OH$	9.04×10^{12}	0	3 080	
187	$C_6H_5CHO + C_6H_5CH_2 \rightharpoonup C_6H_5CO + C_6H_5CH_3$	2.77×10^{3}	2.81	5 773	
188	$C_6H_5CHO + CH_3 \rightharpoonup C_6H_5CO + CH_4$	2.77×10^{3}	2.81	5 773	
189	$C_6H_5CHO + C_6H_5 \rightharpoonup C_6H_5CO + C_6H_6$	7.01×10^{11}	0	4 400	
190	$C_6H_5CO \rightharpoonup C_6H_5 + CO$	4.00×10^{14}	0	29 400	
191	$C_6H_5OH + C_6H_5CH_2 \rightharpoonup C_6H_5O + C_6H_5CH_3$	1.05×10^{11}	0	9 500	

TABLE VII.—COMPARISON OF COMPUTED AND EXPERIMENTAL IGNITION DELAY TIMES FOR TOLUENE OXIDATION BEHIND A REFLECTED SHOCK

Mixture number and description	Initial temperature, T, K	Ignition delay time, τ μs		Percentage difference
		Experimental	Computed	
1	1334	847	975	15.1
Equivalence ratio, φ, 0.331	1353	657	760	15.7
Mole % argon, 85.989	1358	556	702	26.3
Pressure, p, kPa (atm),	1385	388	493	27.1
197.0 to 236.3 (1.95 to 2.34)	1406	287	383	33.4
	1419	221	320	44.8
	1432	186	276	48.4
	1437	183	255	39.3
	1443	124	228	83.9
	----	---	---	[a]42.1
2	1426	1311	1140	–13.0
Equivalence ratio, φ, 1.0	1436	1104	1019	– 7.7
Mole % argon, 95.027	1441	990	948	– 4.2
Pressure, p, kPa (atm),	1496	452	475	5.1
198.0 to 241.4 (1.96 to 2.39)	1505	452	426	– 5.8
	1505	370	430	16.2
	1520	335	364	8.7
	1561	207	218	5.3
	1611	101	120	18.8
	----	----	----	[a]10.7
3	1382	741	870	17.4
Equivalence ratio, φ 1.0	1417	563	580	3.0
Mole % argon, 95.027	1433	490	488	–0.4
Pressure, p, kPa (atm),	1476	330	300	–9.1
566.6 to 674.7 (5.61 to 6.68)	1516	237	190	–19.8
	1520	208	183	–12.0
	1540	175	146	–16.6
	----	---	---	[a]13.1
4	1353	1030	582	–43.5
Equivalence ratio, φ 1.0	1362	975	520	–46.7
Mole % argon, 85.053	1390	596	370	–37.9
Pressure, p, kPa (atm),	1423	356	259	–27.2
236.3 to 293.9 (2.34 to 2.91)	1442	328	208	–36.6
	1483	185	128	–30.8
	1535	100	73	–27.0
	----	----	---	[a]36.4

[a]Standard deviation, σ.

TABLE VIII.—TEMPERATURE DEPENDENCE OF IGNITION DELAY TIMES FOR TOLUENE OXIDATION BEHIND A REFLECTED SHOCK

Mixture number and description	Activation energy factor, ΔE, cal	
	Experimental data	Computed results
1 Equivalence ratio, φ, 0.331 Pressure, p, kPa (atm), ≅ 202 (2)	61 853	50 043
2 Equivalence ratio, φ 1.0 (dilute) Pressure, p, kPa (atm), ≅ 202 (2)	61 774	55 258
3 Equivalence ratio, φ 1.0 (dilute) Pressure, p, kPa (atm), ≅ 606 (6)	38 786	47 872
4 Equivalence ratio, φ 2.0 (strong) Pressure, p, kPa (atm), ≅ 202 (2)	53 256	46 864

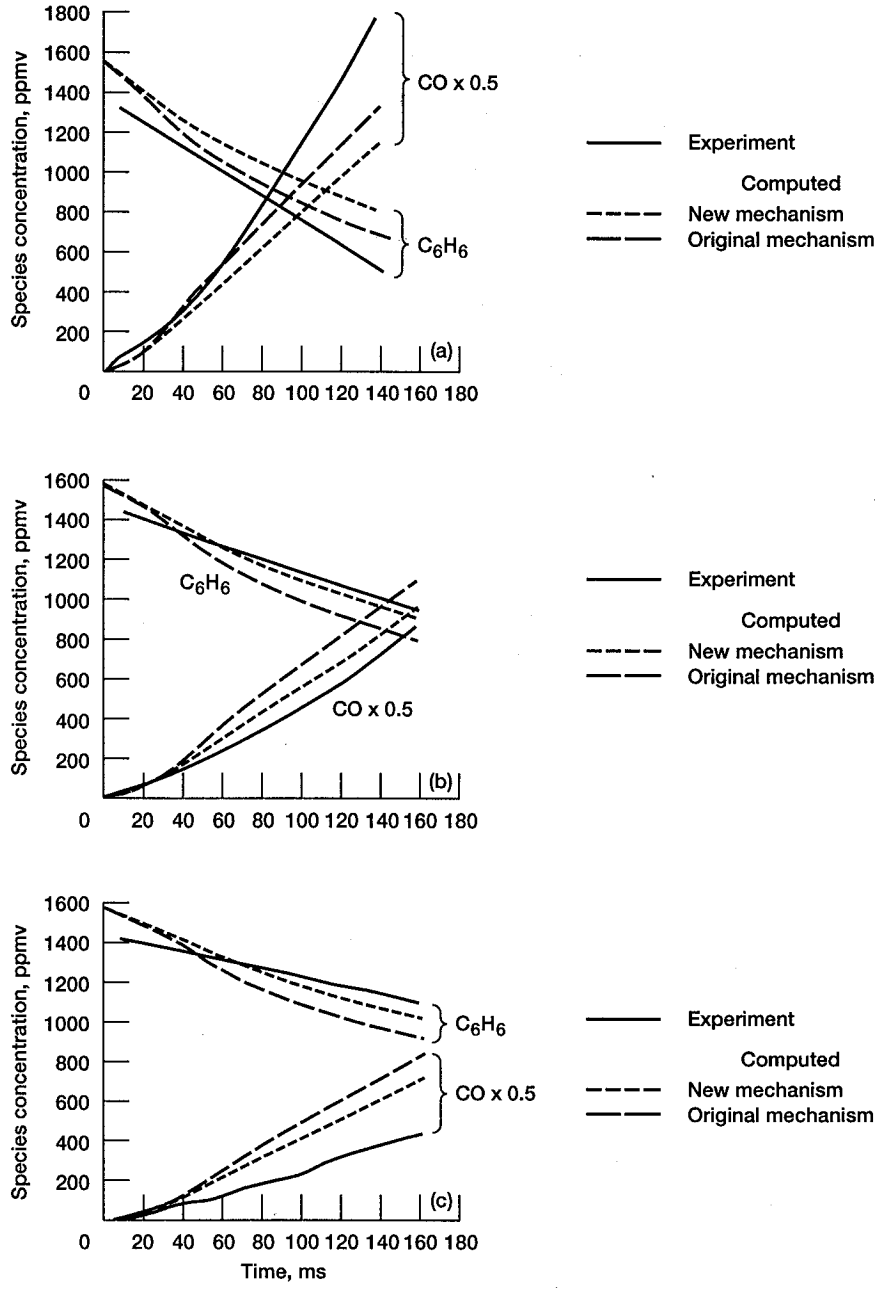

Figure 1.—Concentration time profiles of benzene and carbon monoxide for benzene oxidation in flow reactor. (a) $\varphi = 0.74$; $T_0 = 1098$ K. (b) $\varphi = 1.0$; $T_0 = 1096$ K. (c) $\varphi = 1.36$; $T_0 = 1096$ K.

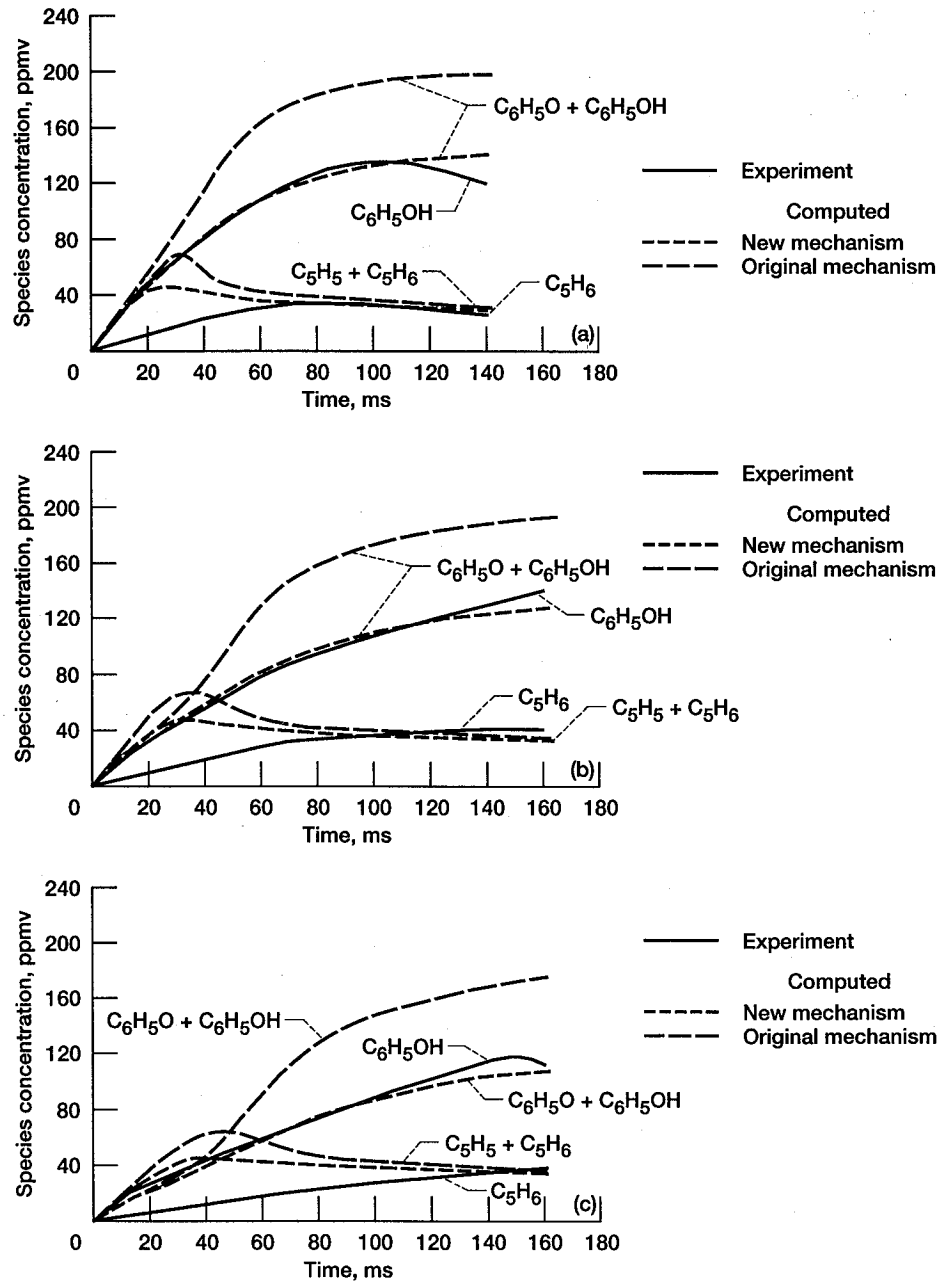

Figure 2.—Concentration time profiles of cyclopentadiene and phenol for benzene oxidation in flow reactor. (a) $\varphi = 0.74$; $T_0 = 1098$ K. (b) $\varphi = 1.0$; $T_0 = 1096$ K. (c) $\varphi = 1.36$; $T_0 = 1096$ K.

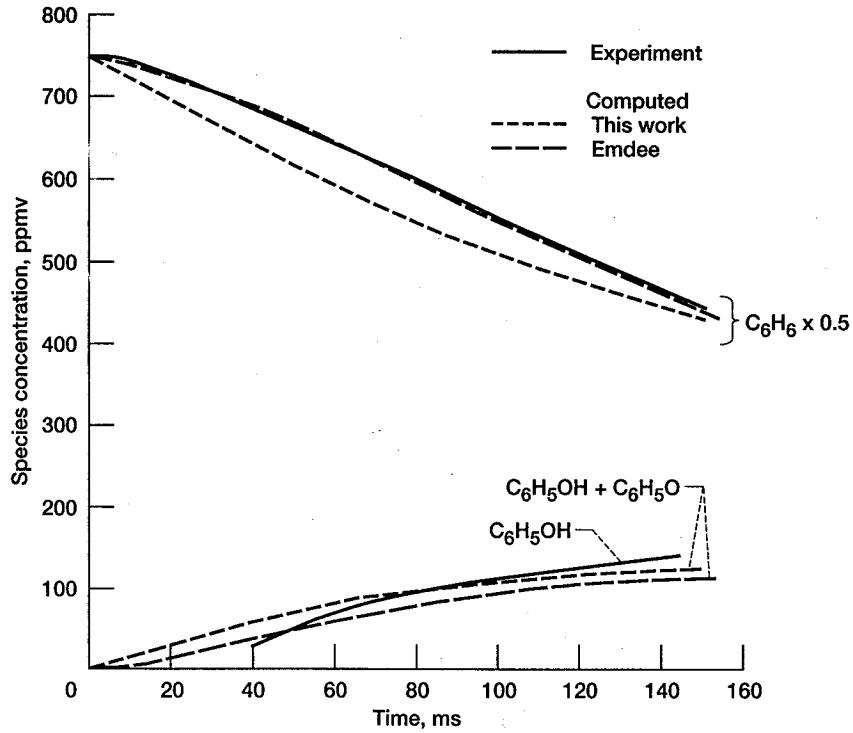

Figure 3.—Concentration time profiles of benzene and phenol for benzene oxidation in flow reactor; $\varphi = 0.91$; $T_0 = 1096$ K.

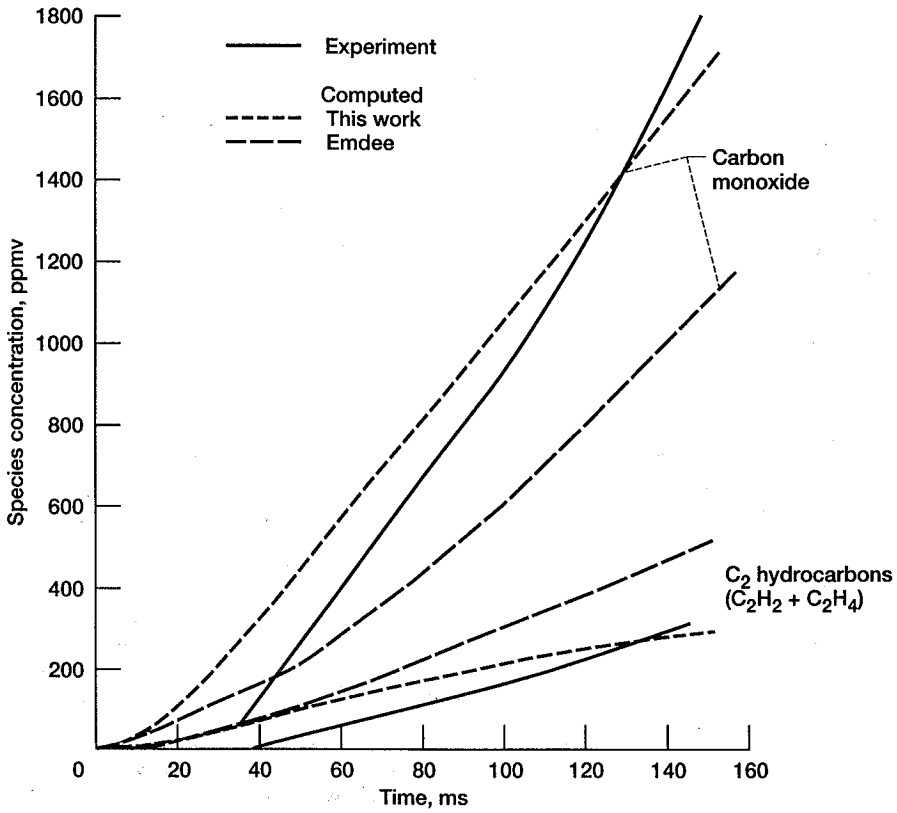

Figure 4.—Concentration time profiles of carbon monoxide and C_2 hydrocarbons for benzene oxidation in flow reactor; $\varphi = 0.91$; $T_0 = 1096$ K.

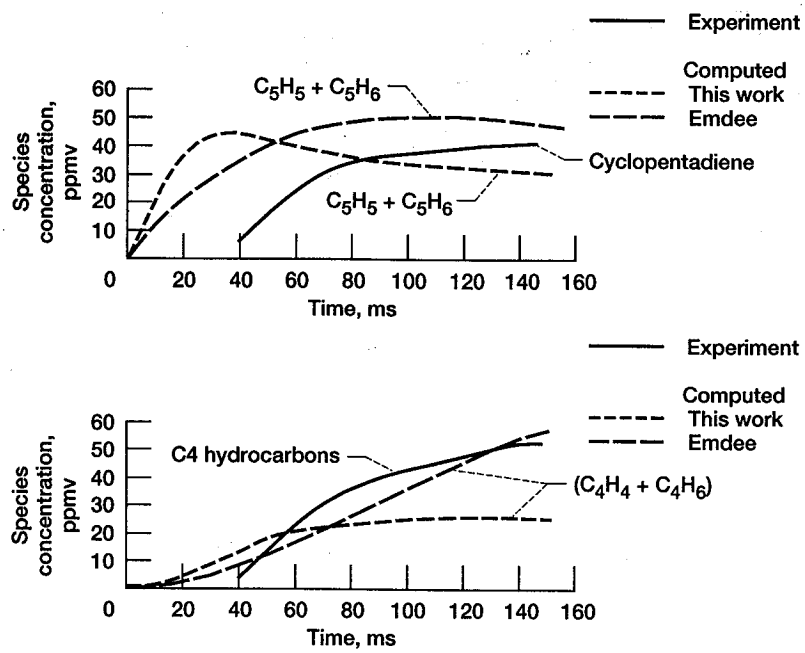

Figure 5.—Concentration time profiles of cyclopentadiene and C_4 hydrocarbons for benzene oxidation in flow reactor; $\varphi = 0.91$; $T_0 = 1096$ K.

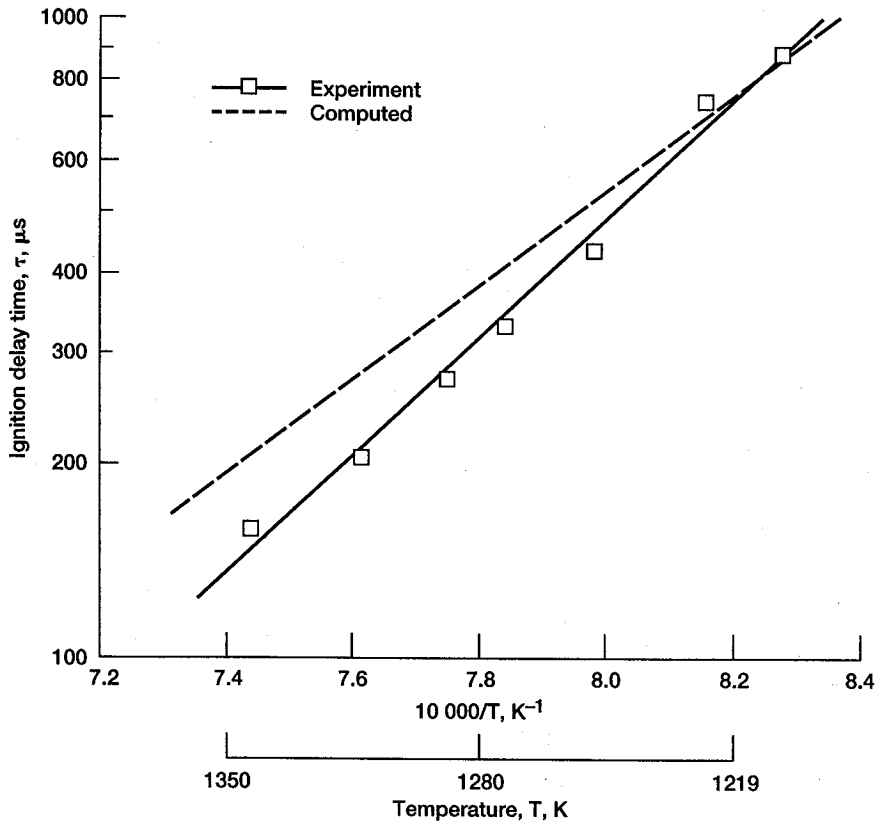

Figure 6.—Ignition delay times for benzene oxidation behind reflected shock; mixture 1; $\varphi = 0.5$; mole % argon = 78.333.

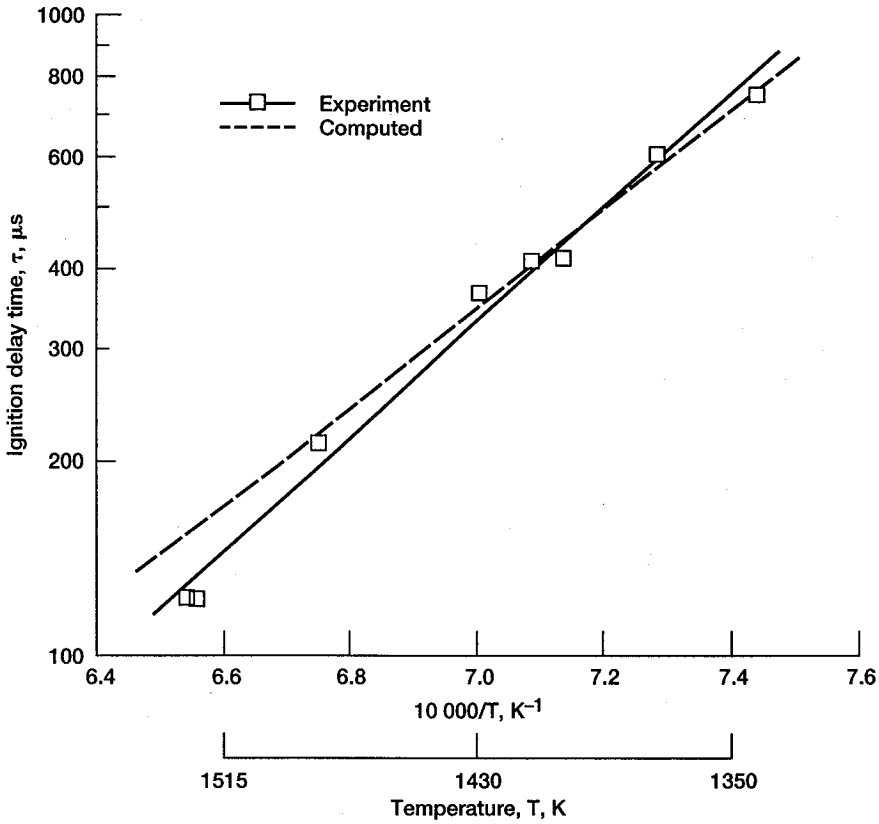

Figure 7.—Ignition delay times for benzene oxidation behind reflected shock; mixture 2, dilute; φ = 1.0; mole % argon = 95.616.

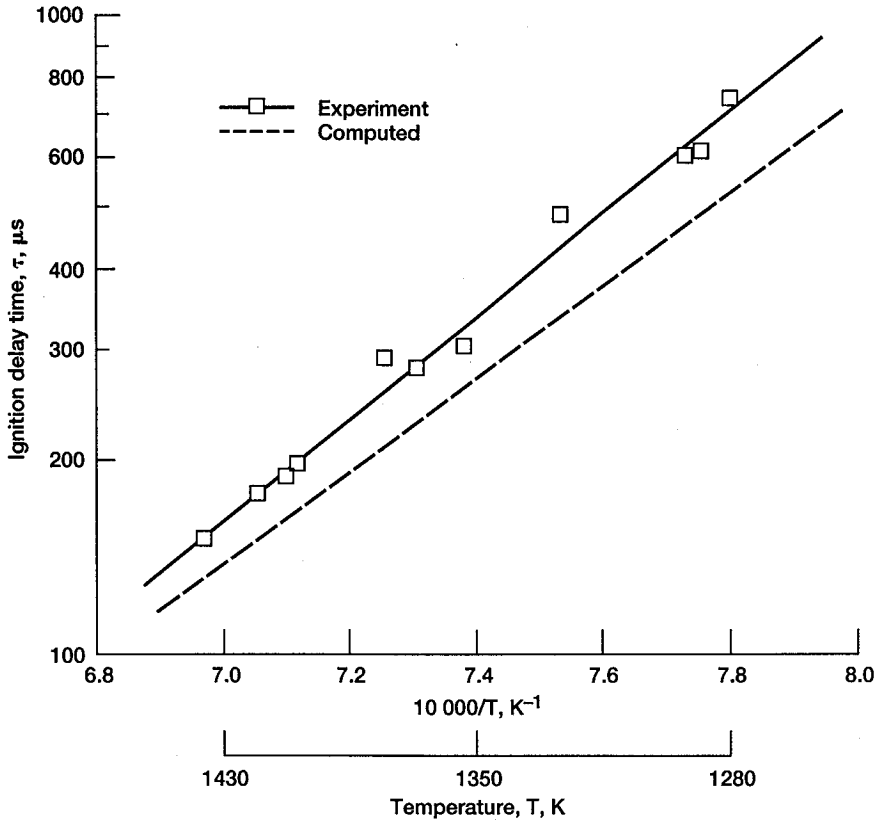

Figure 8.—Ignition delay times for benzene oxidation behind reflected shock; mixture 3, strong; φ = 1.0; mole % argon = 85.635.

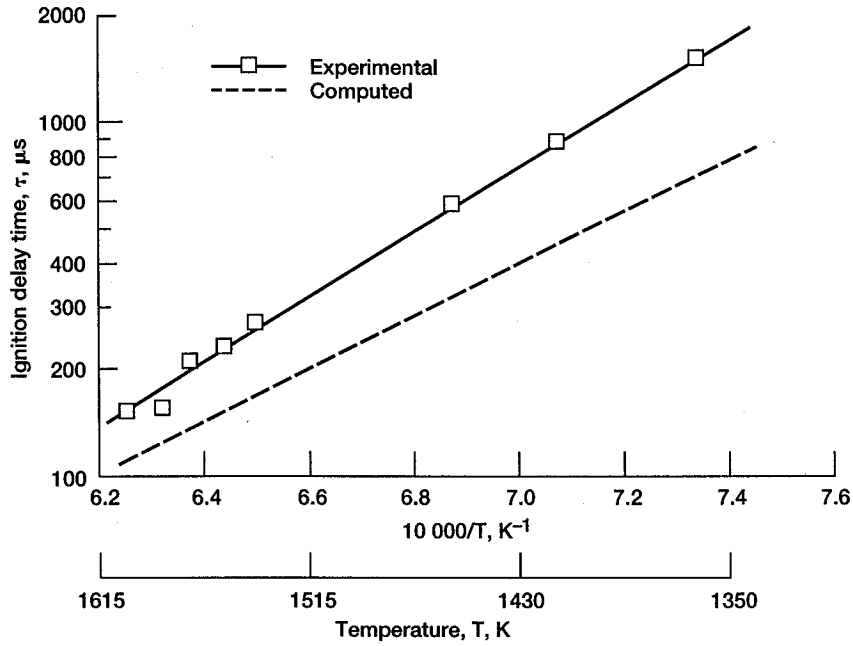

Figure 9.—Ignition delay times for benzene oxidation behind reflected shock; mixture 4; φ = 2.0; mole % argon = 93.553.

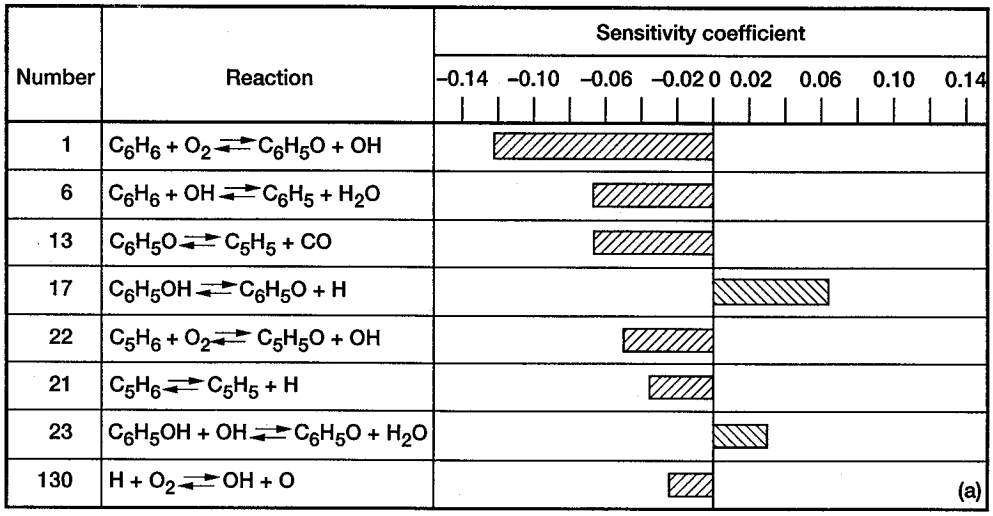

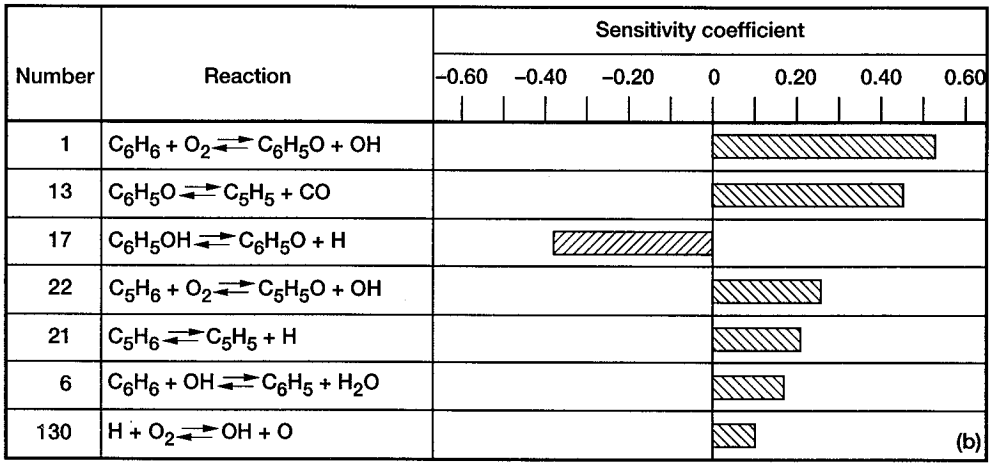

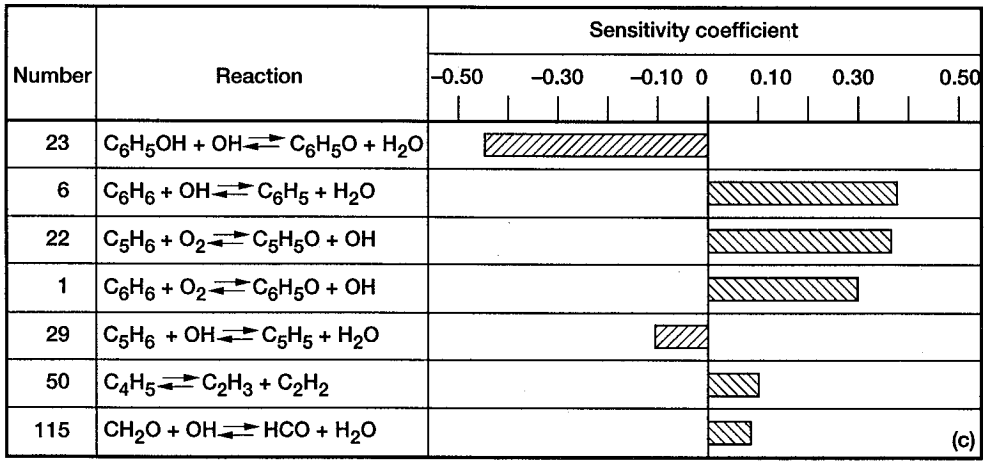

Figure 10.—Sensitivity coefficients for benzene oxidation in flow reactor; $\varphi = 0.74$; $T_0 = 1098$ K; time = 50 ms. (a) Benzene. (b) Carbon monoxide. (c) Phenol.

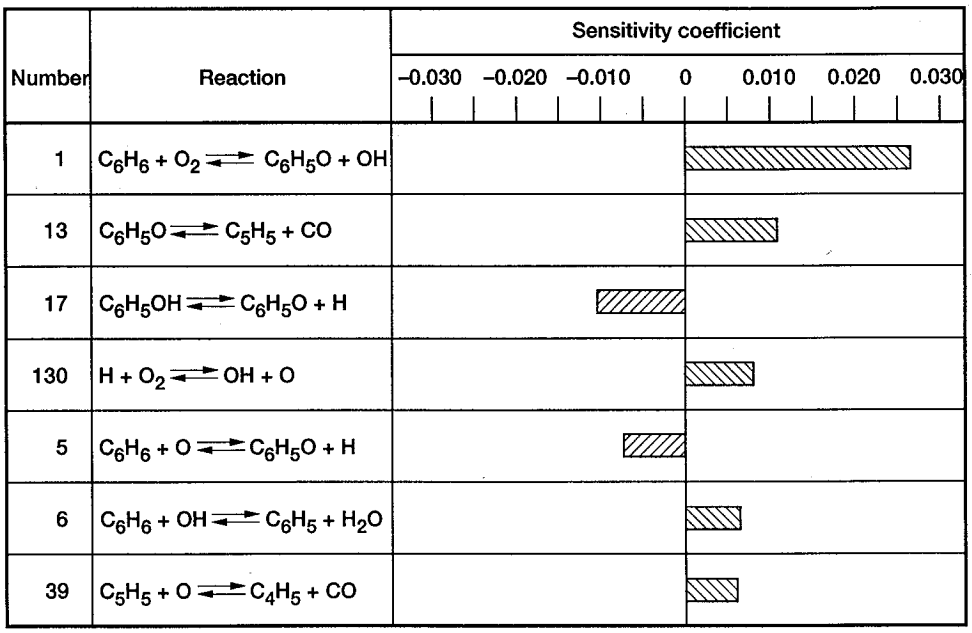

Figure 11.—Sensitivity coefficients for benzene oxidation behind reflected shock; pressure sensitivity; φ = 1.0; mole % argon = 85.093; T_0 = 1435 K; time = 100 μs.

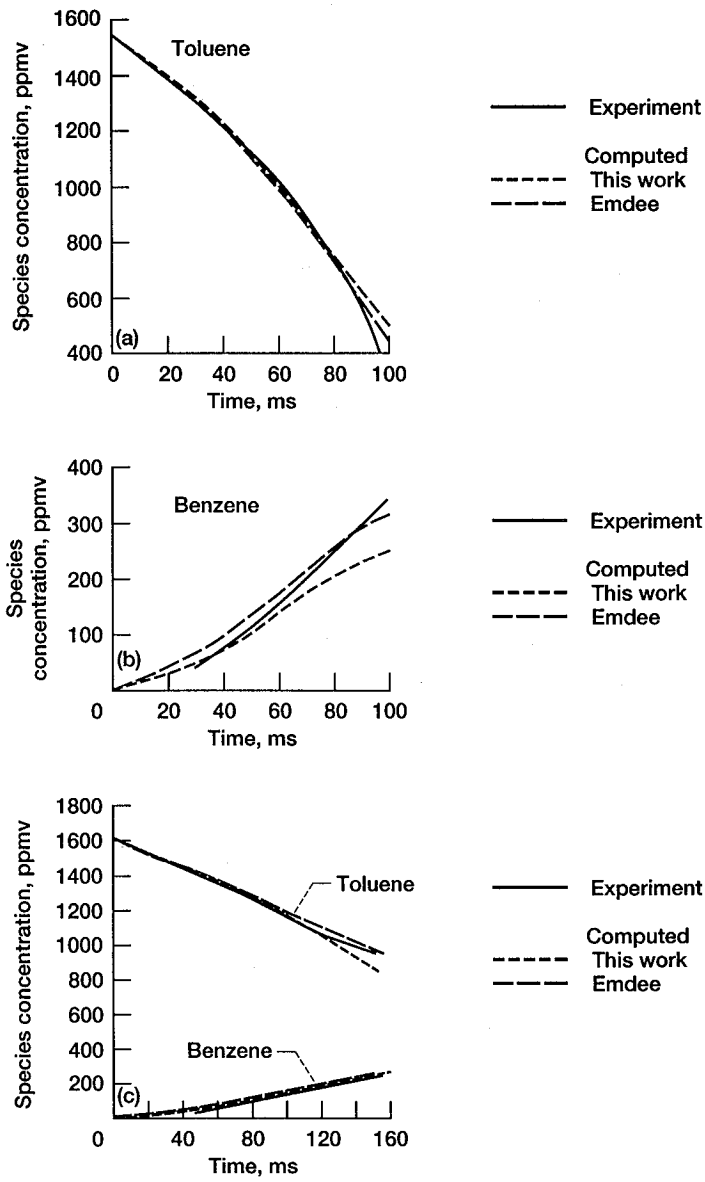

Figure 12.—Concentration time profiles of toluene and benzene for toluene oxidation in flow reactor. (a) and (b) $\varphi = 0.69$; $T_0 = 1188$ K. (c) $\varphi = 1.33$; $T_0 = 1190$ K.

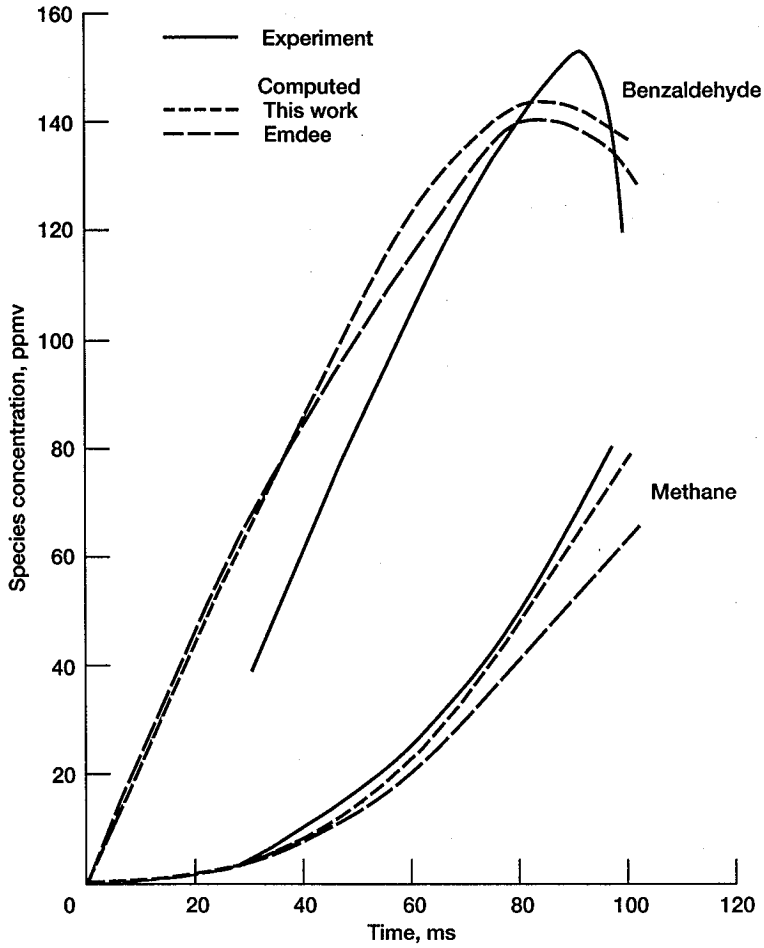

Figure 13.—Concentration time profiles of benzaldehyde and methane for toluene oxidation in flow reactor; $\varphi = 0.69$; $T_0 = 1188$ K.

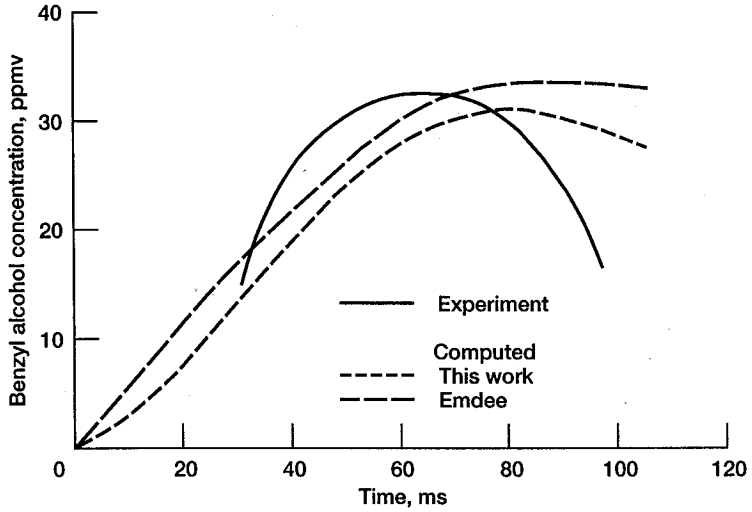

Figure 14.—Concentration time profile of benzyl alcohol for toluene oxidation in flow reactor; $\varphi = 0.69$; $T_0 = 1188$ K.

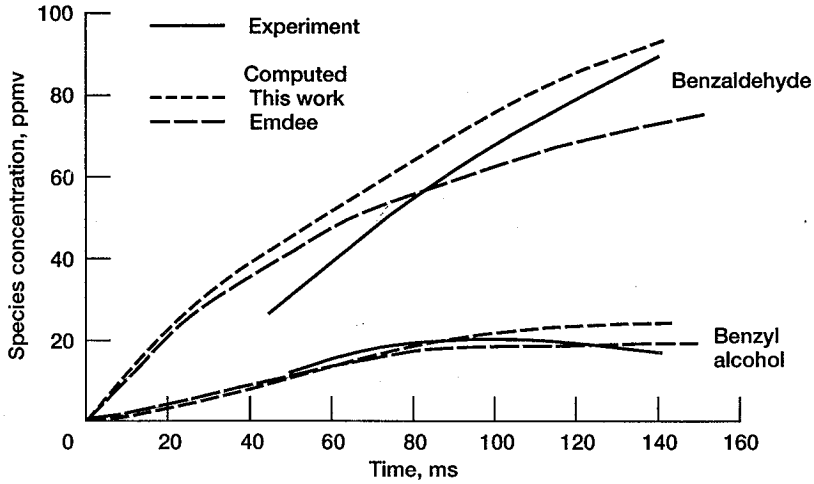

Figure 15.—Concentration time profiles of benzaldehyde and benzyl alcohol for toluene oxidation in flow reactor; $\varphi = 1.33$; $T_0 = 1190$ K.

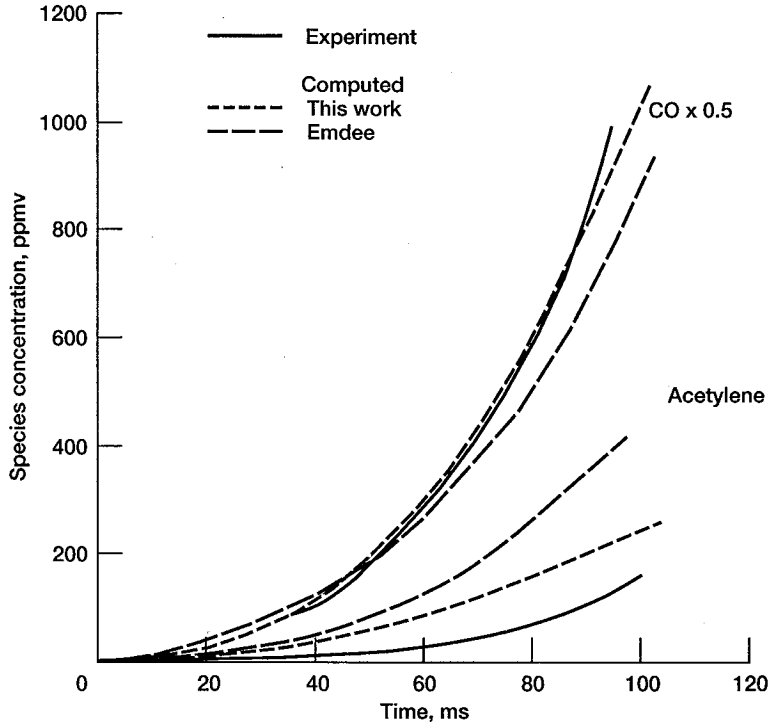

Figure 16.—Concentration time profiles of carbon monoxide and acetylene for toluene oxidation in flow reactor; $\varphi = 0.69$; $T_0 = 1188$ K.

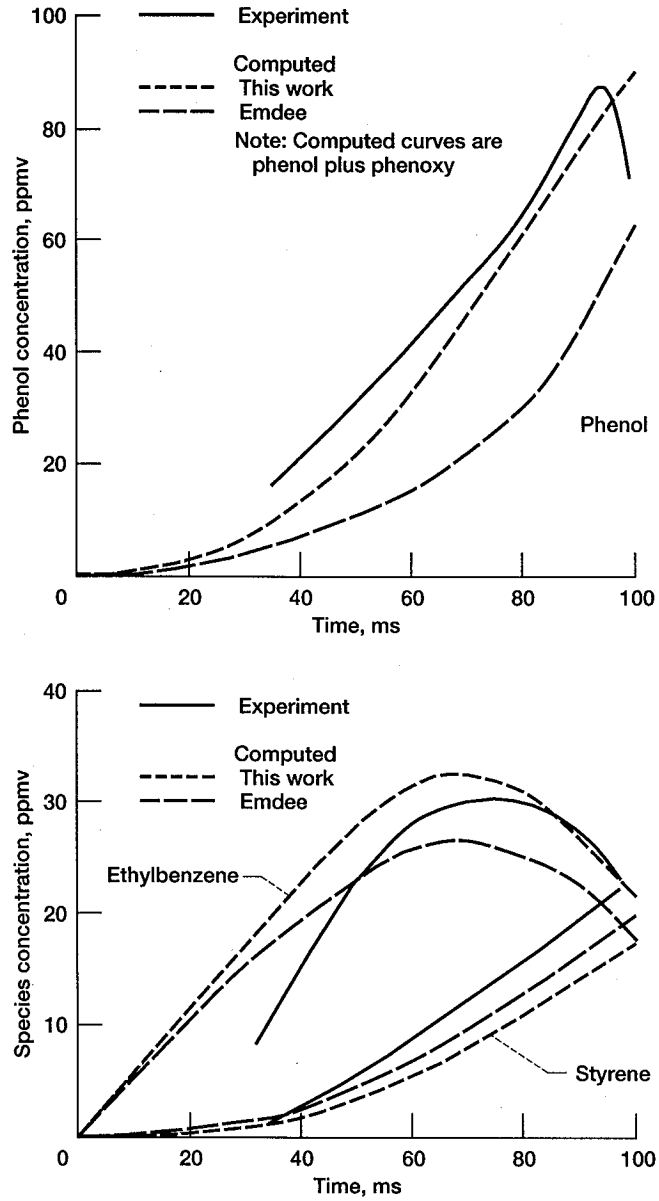

Figure 17.—Concentration time profiles of phenol, ethylbenzene, and styrene for toluene oxidation in flow reactor; $\varphi = 0.69$; $T_0 = 1188$ K.

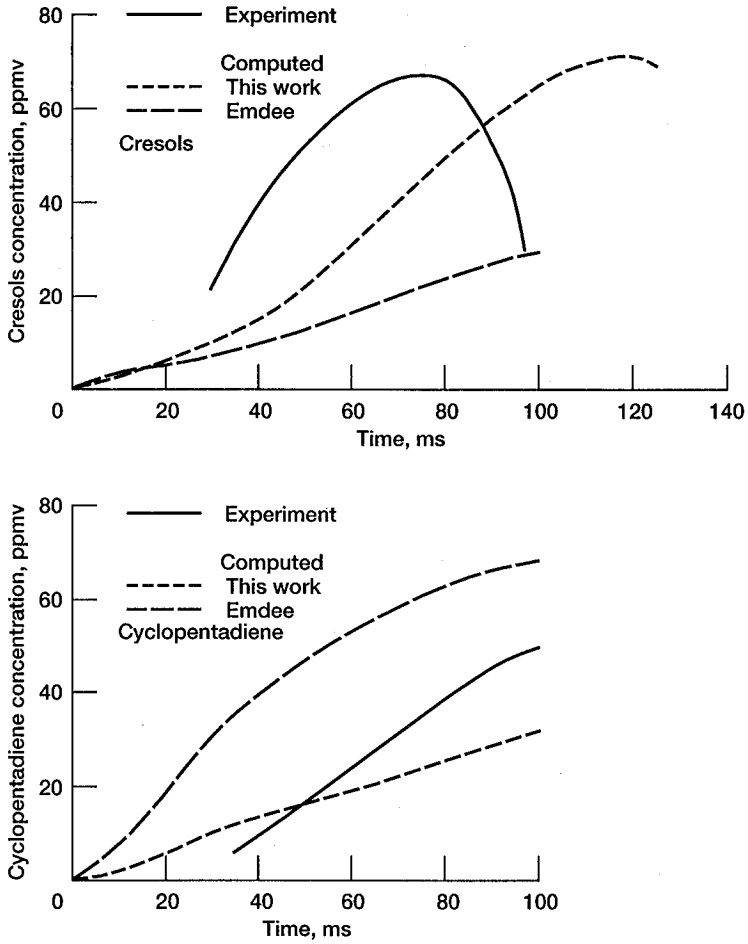

Figure 18.—Concentration time profiles of cresols and cyclopentadiene for toluene oxidation in flow reactor; $\varphi = 0.69$; $T_0 = 1188$ K.

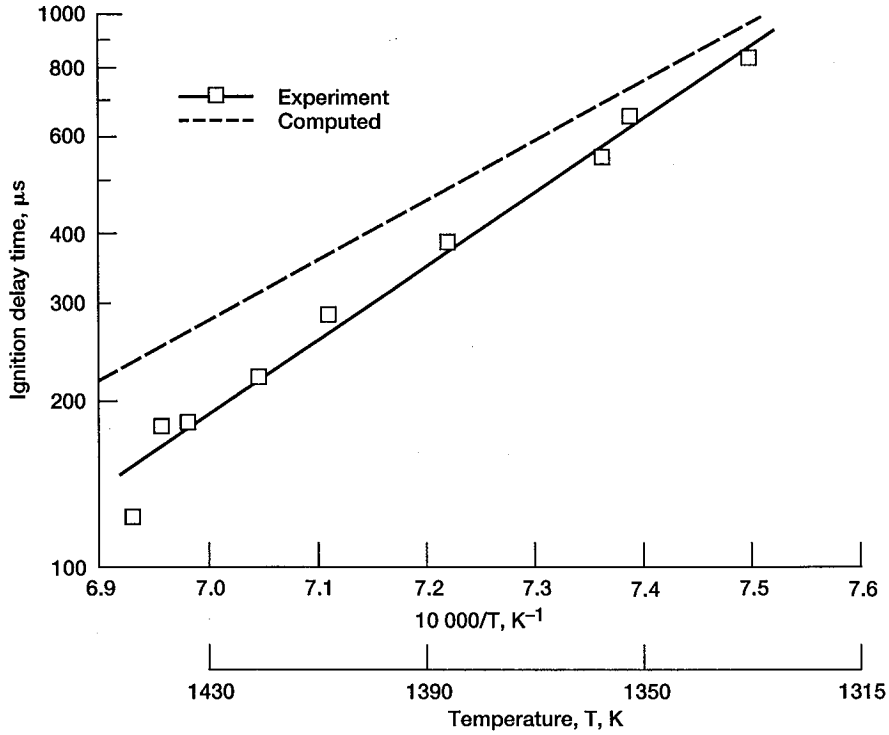

Figure 19.—Ignition delay times for toluene oxidation behind reflected shock; mixture 1; $\varphi = 0.331$; pressure ≅ 202 kPa (≅ 2 atm).

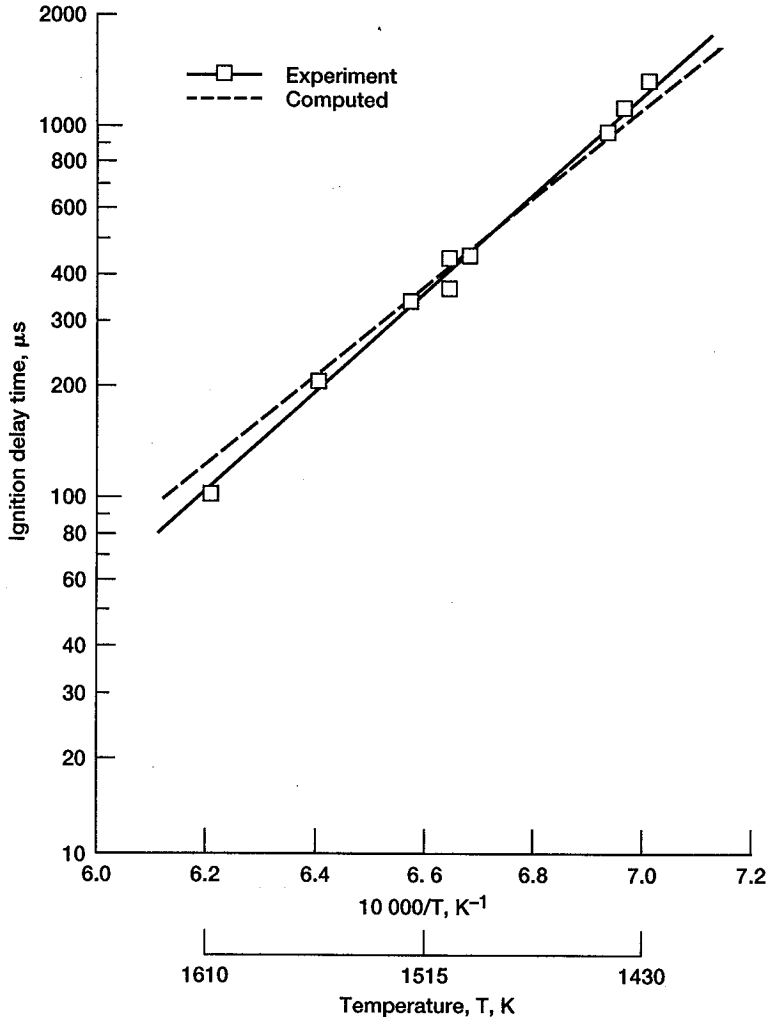

Figure 20.—Ignition delay times for toluene oxidation behind reflected shock; mixture 2; $\varphi = 1.0$; mole % argon = 95.207; pressure ≅ 202 kPa (≅ 2 atm).

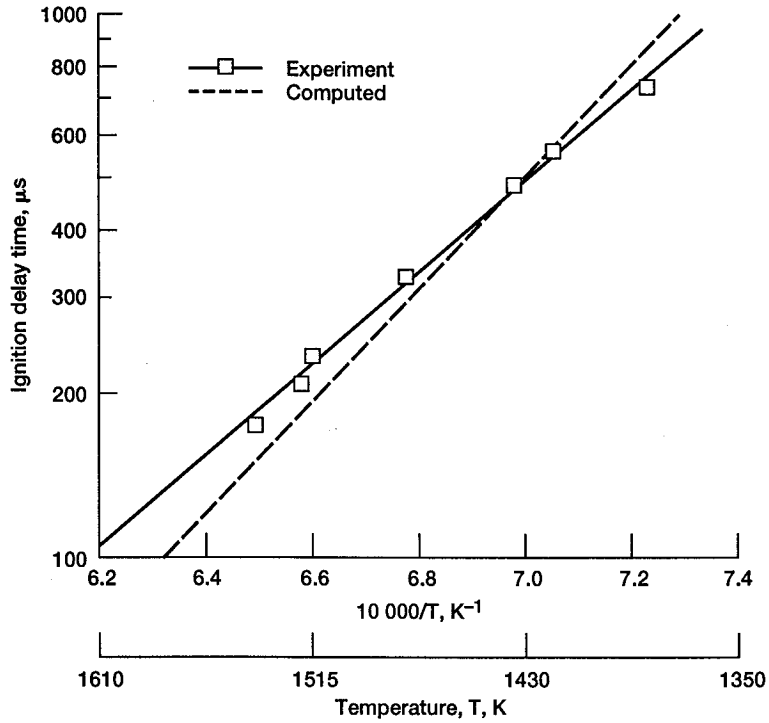

Figure 21.—Ignition delay times for toluene oxidation behind reflected shock; mixture 3; φ = 1.0; mole % argon = 95.207; pressure ≅ 606 kPa (≅ 6 atm).

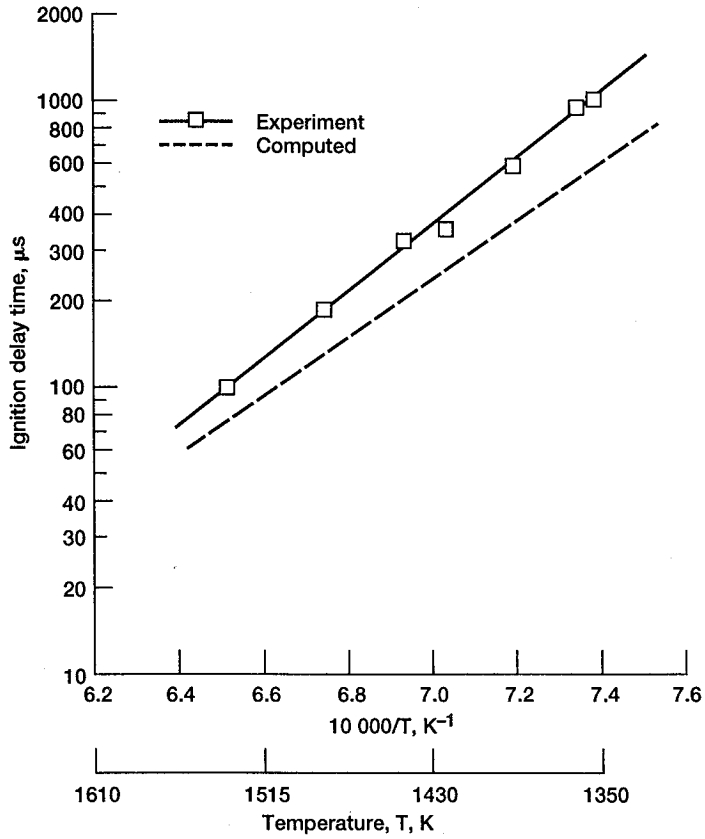

Figure 22.—Ignition delay times for toluene oxidation behind reflected shock; mixture 4; φ = 1.0; mole % argon = 85.053; pressure ≅ 202 kPa (≅ 2 atm).

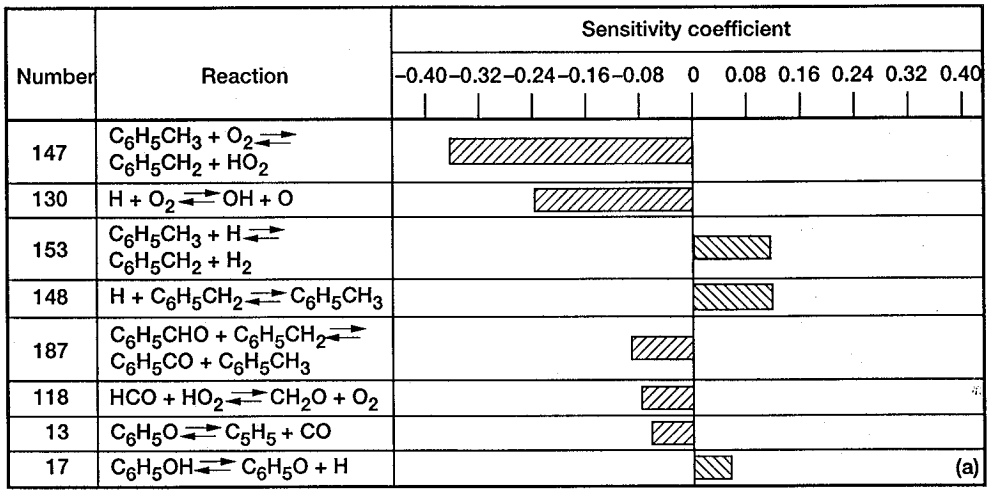

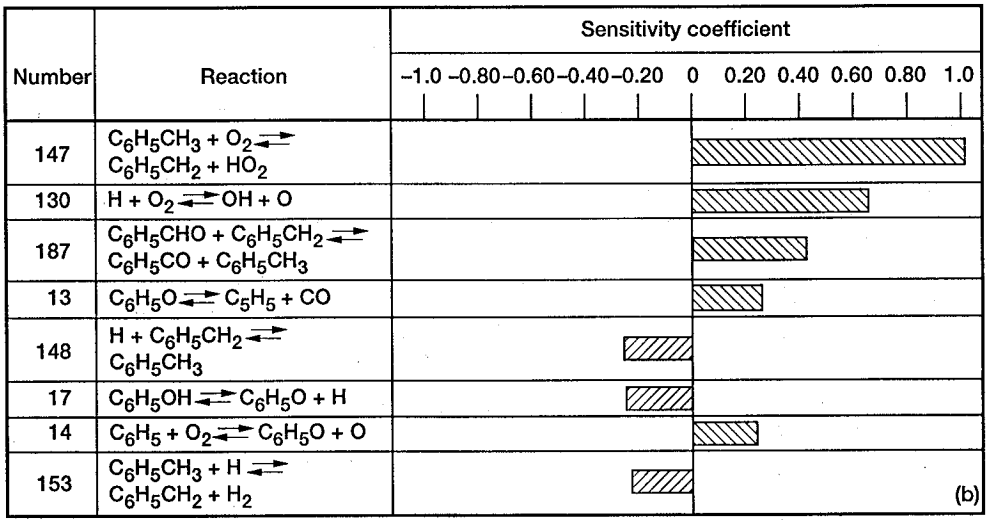

Figure 23.—Sensitivity coefficients for toluene oxidation in flow reactor; $\varphi = 0.69$; $T_0 = 1188$ K; time = 60 ms. (a) Toluene. (b) Carbon monoxide.

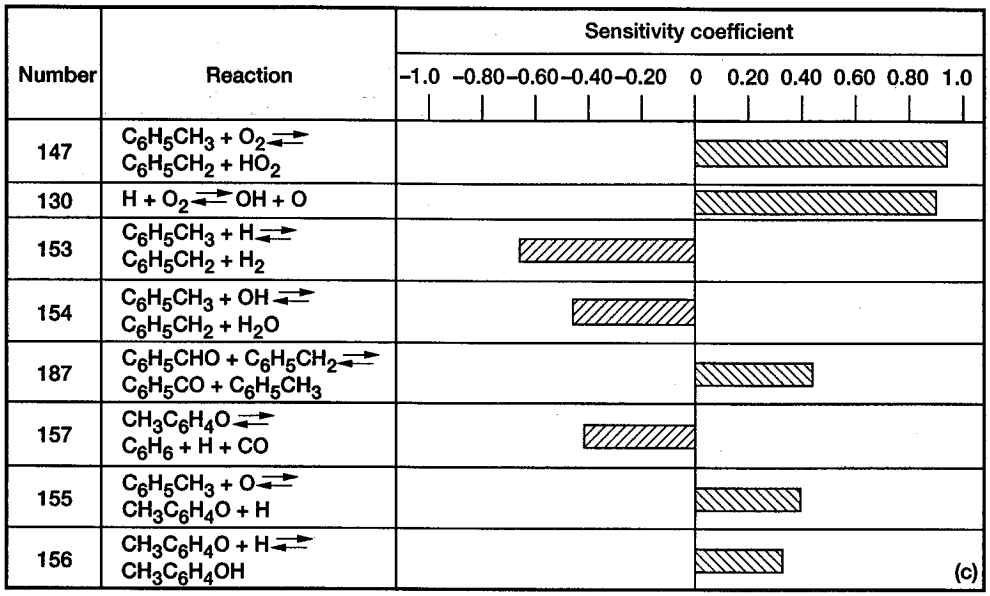

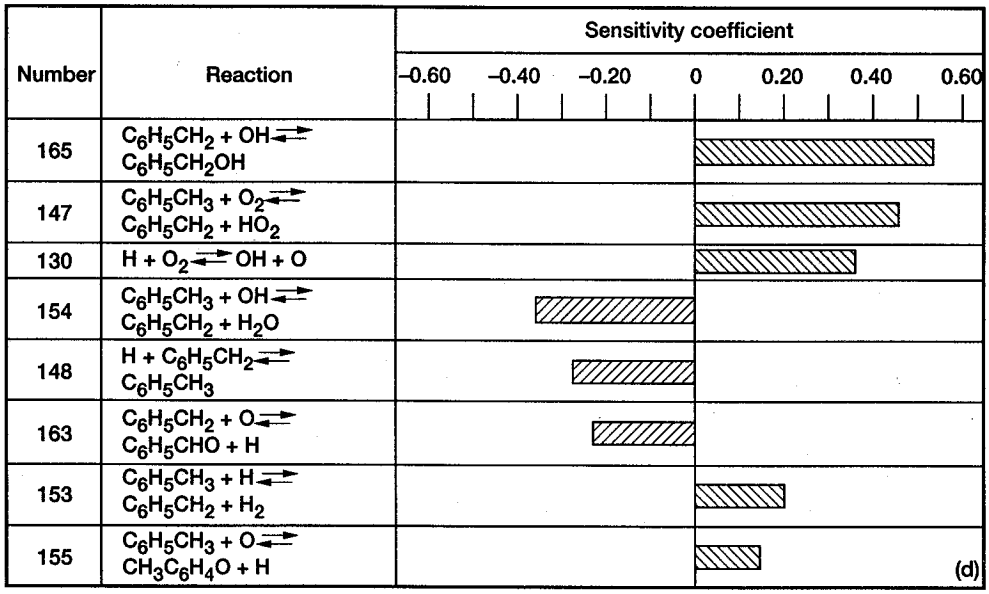

Figure 23.—Concluded. (c) Cresol. (d) Benzyl alcohol.

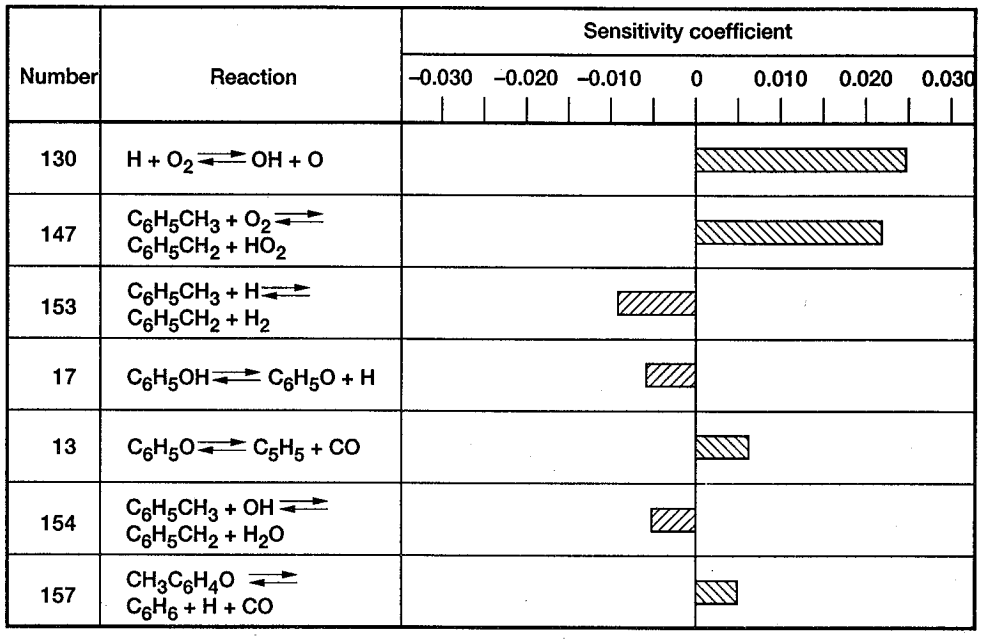

Figure 24.—Sensitivity coefficients for toluene oxidation behind shock wave; pressure sensitivity; $\varphi = 0.331$; $T_0 = 1334$ K; time = 700 μs.

REPORT DOCUMENTATION PAGE

Form Approved
OMB No. 0704-0188

1. AGENCY USE ONLY (*Leave blank*)	2. REPORT DATE	3. REPORT TYPE AND DATES COVERED
	December 1995	Technical Paper

4. TITLE AND SUBTITLE

Oxidation Mechanisms of Toluene and Benzene

5. FUNDING NUMBERS

WU–505–62–52

6. AUTHOR(S)

David A. Bittker

7. PERFORMING ORGANIZATION NAME(S) AND ADDRESS(ES)

National Aeronautics and Space Administration
Lewis Research Center
Cleveland, Ohio 44135–3191

8. PERFORMING ORGANIZATION REPORT NUMBER

E–9015–1

9. SPONSORING/MONITORING AGENCY NAME(S) AND ADDRESS(ES)

National Aeronautics and Space Administration
Washington, D.C. 20546–0001

10. SPONSORING/MONITORING AGENCY REPORT NUMBER

NASA TP–3546

11. SUPPLEMENTARY NOTES

Responsible person, David A. Bittker, organization code 2650, (216) 433–5911.

12a. DISTRIBUTION/AVAILABILITY STATEMENT

Unclassified - Unlimited
Subject Categories 25 and 28

This publication is available from the NASA Center for Aerospace Information, (301) 621–0390.

12b. DISTRIBUTION CODE

13. ABSTRACT ***(Maximum 200 words)***

An expanded and improved version of a previously published benzene oxidation mechanism is presented and shown to model published experimental data fairly successfully. This benzene submodel is coupled to a modified version of a toluene oxidation submodel from the recent literature. This complete mechanism is shown to successfully model published experimental toluene oxidation data for a highly mixed flow reactor and for higher temperature ignition delay times in a shock tube. A comprehensive sensitivity analysis showing the most important reactions is presented for both the benzene and toluene reacting systems. The NASA Lewis toluene mechanism's modeling capability is found to be equivalent to that of the previously published mechanism which contains a somewhat different benzene submodel.

14. SUBJECT TERMS	15. NUMBER OF PAGES
Aromatic hydrocarbon oxidation; Reaction mechanisms; Complex chemical kinetic computations; Sensitivity analysis	46
	16. PRICE CODE: A03

17. SECURITY CLASSIFICATION OF REPORT	18. SECURITY CLASSIFICATION OF THIS PAGE	19. SECURITY CLASSIFICATION OF ABSTRACT	20. LIMITATION OF ABSTRACT
Unclassified	Unclassified	Unclassified	